

# HF Meteor Trail Reflections Observed at Anchorage, Alaska USA

Whitham D. Reeve

## 1. Introduction

Many interesting phenomena can be observed in the high frequency (HF) radio band including *meteor trail reflections*, radio blackouts and sudden frequency deviations (see {[Reeve15-1](#)} and {[Reeve15-2](#)}), aurora reflections, aircraft reflections, and propagation anomalies due to ionospheric patches and blobs. Detections of all these phenomena at Anchorage, Alaska involve a terrestrial transmitter and terrestrial receiver separated by a distance great enough to result in sky wave propagation between them.



This article focuses on meteor trail reflections. The transmissions originate at distant transmitters, are reflected by the ionized trails left by tiny meteors as they vaporize in Earth's upper atmosphere, and are detected by a receiver (figure 1). Other names for meteor trail reflections seen in the literature are *meteor echoes*, *meteor scatter*, *meteor propagation* and *radio meteors*.

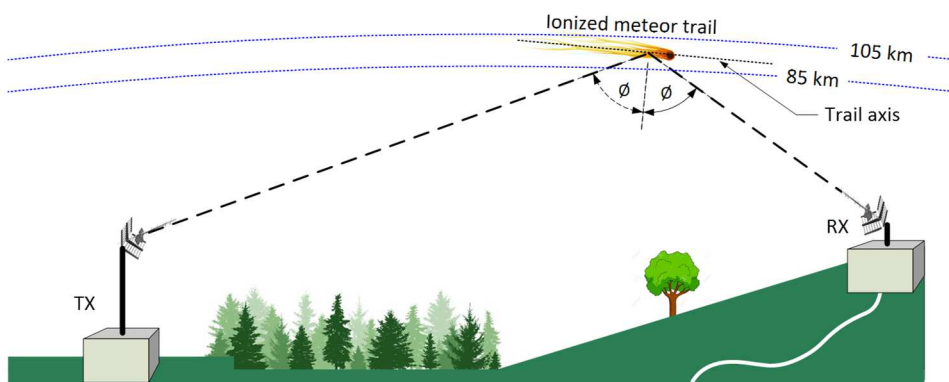


Figure 1 ~ Simplified 2-dimensional drawing of a meteor trail reflection propagation path. The plane of propagation that includes transmitter TX, meteor trail and receiver RX may be tilted and not vertical as implied here. The incident and reflection angles to the trail axis are the same and indicated by the symbol  $\phi$ . Image © 2020 W. Reeve

Included in this article are a brief overview of the concepts that underly the observations of meteor trail reflections (section 2), considerations for observations (section 3), instrumentation used to receive the reflections at Anchorage (section 4), a selection of spectrum images from 2020 showing meteor trail reflections (section 5), conclusions (section 6), and references and weblinks (section 7).

I started an overall project in 2014 to try to understand HF propagation at higher latitudes (my receiver station is at N62° magnetic on the southern edge of the auroral oval). I decided to use the transmissions from the distant WWV and WWVH time-frequency stations because they have very high accuracy and reliability. My initial plan was to determine if these transmissions are reflected by meteor trails and then detectable at my Anchorage observatory. That led to trying to understand the spectra received from that propagation, which included many more features than just meteor trail reflections.

This effort was (and still is) successful, but, because of my inexperience, I did not immediately recognize the meteor trail reflection spectra signatures produced by my monitoring software. However, in early 2019 I read a professional paper [Bourdillon] that included some spectra of HF meteor trail reflections almost identical to

what I had recorded. Not long after that, I contacted a regular contributor of radio meteor reports in MeteorNews {[MetNews](#)}, who verified some of my spectra images.

I have not attempted to count the number of detected meteor trails or determine their peak times and dates as is often done by other observers. I do attempt in section 5 to assign the various detections to particular meteor showers. I used the meteor calendars produced by the International Meteor Organization {[IMOMC](#)} as a guide. However, I do not know the shower radiants and because some showers overlap, my assignments during those periods may be wrong. I did not detect some major showers probably because the needed propagation geometry or ionospheric conditions did not exist during those times.

Near real-time Argo spectrograms produced by my system at Anchorage are posted at {[Meteor](#)}. The Argo software {[Argo](#)} is used for this purpose, and it produces a narrowband spectrogram every 12 min. All of the images are archived (over 300 000 as of 31 December 2020). The recorded spectra are quite varied and include not only meteor trail reflections but also the other phenomena mentioned above. Many archive images are blank because no propagation by any means existed between the transmitter and receiver stations. All spectra are subject to interpretation, and it is possible my interpretations are incorrect in some cases. For example, it is possible that sporadic-E or aurora reflections are involved in some situations. Reader feedback is welcome (see contact information at the end).

My Anchorage observatory is not the only station that posts near real-time spectrograms showing meteor trail reflections and other phenomena. For example, in New Mexico, the Roswell Meteor website at {[Roswell](#)} posts Argo spectra associated with WWV on 25 MHz and other frequencies and sources. In the Washington, DC area {[LiveMeteor](#)} posts real-time audio associated with reflections of a television station video carrier.

---

## 2. Meteor Trail Reflection Concepts

The numerical information in this section is from [Goodman], [McKinley], [Schanker] and [Sugar]. It is estimated that trillions of tiny meteors – dust grains – enter Earth’s upper-atmosphere each day. The particles of interest have masses ranging from  $10^{-7}$  to  $10^{-1}$  g and diameters ranging from 2  $\mu\text{m}$  to 2 mm (figure 2). The mass distribution is such that there are approximately equal total masses of each particle size. For example, there are 10-times as many particles with mass  $10^{-4}$  g as there are particles with mass  $10^{-3}$  g.

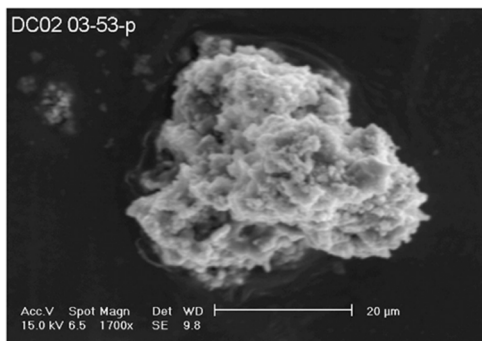


Figure 2 ~ Fine-grained, *fluffy* micrometeorite that survived atmospheric entry and was later found in Antarctica. An unknown fraction of micrometeoroids actually make it to the ground. The particle is approximately 40  $\mu\text{m}$  wide. This image is from a scanning electron microscope. Image source: [Duprat]

The speeds of the particles range from about 11 to 72 km s<sup>-1</sup>. The lower limit is the lowest velocity that a particle falling toward Earth can have and is equal to the escape velocity of a body leaving Earth. The upper limit has two components. One is the speed of Earth in its orbit around the Sun, which is about 30 km s<sup>-1</sup>, and the other is the escape velocity of a body leaving the Sun in the vicinity of Earth, which is about 42 km s<sup>-1</sup>. Escape velocity  $v_e$  may be calculated from

$$v_e = \sqrt{2 \cdot G \cdot M / r} \quad (1)$$

where  $G$  is the universal gravitational constant ( $6.67 \cdot 10^{-11} \text{ m}^3 \text{ kg}^{-1} \text{ s}^{-2}$ ),  $M$  is the mass of the body from which the object is escaping or falling toward (kg) and  $r$  is the distance from the center of mass of the body to the object (m). For Earth's escape velocity,  $M_E \approx 6 \cdot 10^{24} \text{ kg}$  and  $r \approx 6.470 \cdot 10^6 \text{ m}$  (Earth's radius  $R_E$  + 100 km reflection height), and for the Sun's escape velocity at Earth's distance,  $M_S \approx 2 \cdot 10^{30} \text{ kg}$  and  $r \approx 150 \cdot 10^9 \text{ m}$ .

The meteor particle's kinetic energy is converted to heat by friction as it collides with the atoms and molecules in Earth's atmosphere. The heat is intense enough to vaporize the surface atoms of the meteor in a process called *ablation*. These ablated atoms are ionized and leave a trail, or column, of positively charged ions and free electrons. The heat also may break the meteor into smaller particles. It is estimated that between 100 and 1000 tons of this dust enter Earth's atmosphere each day and more than 5000 tons fall to Earth each year.

The ionized meteor trail is a long thin paraboloid, typically 50 km long, with the meteor particle at its head. The ions do not interact with radio waves because of their relatively high mass but the much lighter free electrons readily react at radio frequencies. The higher the meteor's mass, the higher the electron density in a line along the meteor's path, ranging from  $10^{10}$  to  $10^{16}$  electrons m<sup>-1</sup>. This density is far higher than in the surrounding ionosphere, and it is this dense line of free electrons that interacts with the radio wave.

Meteor trails are categorized as *underdense* and *overdense*. Underdense meteor trails are far more common by an estimated ratio of 20:1. The commonly used line density threshold between underdense and overdense trails is  $10^{14}$  electrons m<sup>-1</sup>. In underdense trails, the radio wavefront penetrates the ionized trail and is scattered *coherently* (in phase) by the free electrons. The resulting radio wave is the sum of the scattered fields from individual electrons. This process is most efficient at VHF but the scattering also occurs with radio waves at HF (as will be shown later). The excited electrons scatter the incident radio wave at an angle equal but opposite to the incident angle (see figure 1).

Meteor particles associated with overdense trails are larger and their trails have much higher electron densities. The density is so great that the radio waves do not penetrate the trail but, instead, are reflected by it (specular reflection). In this article, the terms *reflection* and *echo* will be used interchangeably regardless of the mechanism involved in the radio wave's interaction with the meteor trail. The spectrograms of some individual long-duration echoes appear to show head echoes, which is a brighter thin line, usually curved, at the beginning of the reflection. These are thought to be reflections from the ionization produced by intense ultraviolet radiation at some distance from the meteor head.

The reception of meteor trail reflections involves a form of bistatic radar in which the transmitter and receiver are at fixed locations but separated by some distance. In this article, the WWV and WWVH stations near Fort Collins in Colorado and near Kekaha on the Island of Kauai in Hawaii, respectively, are the transmitters and the

receiver is in southcentral Alaska at Anchorage. The WWV transmitters are approximately 3800 km east-southeast and the WWVH transmitters are 4400 km south-southwest of Anchorage (figure 3). The distances are great enough to ensure that at least two hops are needed to receive the signals at Anchorage via sky waves (propagation modes are discussed in more detail in section 3).

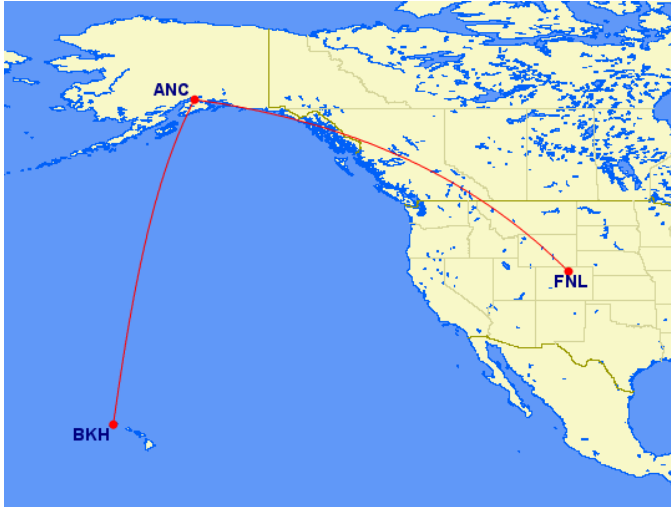


Figure 3 ~ Great circle paths shown in red between WWV near Fort Collins, Colorado (marked FNL) and my observatory in Anchorage, Alaska (ANC) and between WWVH near Kekaha on Kauai, Hawaii (BKH) and Anchorage. The paths are long enough to require multi-hop propagation. The WWVH path is almost entirely over water and encounters different propagation conditions than the WWV path, which is entirely over land. Anchorage is at the southern edge of the auroral oval, which introduces additional factors in the HF radio propagation. Image from {GCMaP}.

It is not necessary that the distances from the receiver and transmitter to the reflection point be equal but their line-of-sight distances are limited by Earth’s curvature to  $R_{max}$  determined from

$$R_{max} = 2 \cdot R_E \cdot \arccos[R_E / (R_E + H)] \cdot (\pi/180) \text{ km} \tag{2}$$

where  $R_E$  is Earth’s radius (km, approximately 6370 km) and  $H$  is the reflection height or altitude above ground level (km). If the result of the arc-cosine calculation in equation (2) is in degrees, the factor  $\pi/180$  is needed to convert the result to radians for the distance calculation. If the result already is in radians, the factor is not needed.

Meteor trail reflections occur in a fairly narrow altitude range of approximately 85 km to 105 km, corresponding to the region where the mesosphere transitions to the thermosphere in Earth’s atmosphere; This range also corresponds to the upper D-region and lower E-region of the ionosphere. The theoretical altitude range is from 80 to about 120 km. Most particles are completely vaporized before reaching 80 km altitude. Generally, the higher the meteor velocity, the higher the altitude at which its ionized trail is detected. For meteor trail altitudes of 85 and 105 km,  $R_{max}$  from equation (2) is 2070 and 2297 km, respectively.

Generally, line-of-site paths from the transmitter to the meteor trail and from the meteor trail to the receiver are necessary for reception of frequencies above roughly 40 MHz, such as those from television and FM broadcast band transmitters. At lower frequencies and long distances the signals are refracted by the ionosphere and reflected by the ground, so that multi-hop propagation modes are involved.

For multi-hop HF propagation paths around 4000 km, equation (2) is not used on the entire path but it can be used for individual hops. For example, say propagation involves 2 hops with a total great circle distance of 4000 km. Each hop would be 2000 km assuming equal distances between ground reflection points. In this case, the

hop closest to the receiver would be within the approximate 2000 km maximum calculated above. As will be shown later, 3-hop and higher mode paths are more likely for the situations covered in this article.

To explain meteor trail reflections from transmitters on the order of 4000 km away, the ground reflection and ionosphere refraction points nearest the receiver could be considered the locations of virtual transmitters (figure 4).

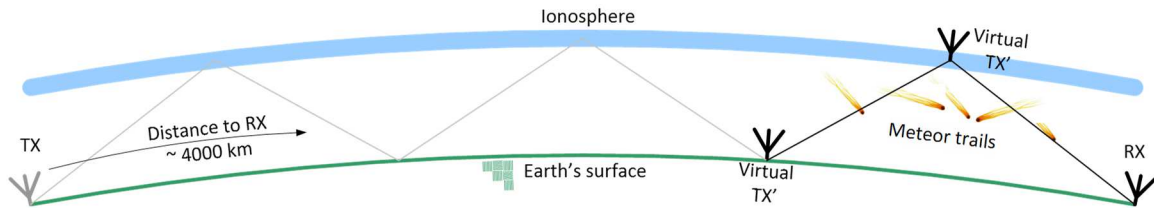


Figure 4 ~ 3-hop propagation path shown with two virtual transmitter TX' locations on the hop nearest the receiver Rx; one or both may exist. The virtual transmitters are used to explain how signals from the distant WWV and WWVH transmitters can be reflected off meteor trails and detected at the Anchorage observatory. The radio waves from the virtual transmitters are reflected by a meteor trail by forward scatter to the receiver but back scatter also may occur.

The received signal level depends on many factors such as transmitter power and frequency, receiver sensitivity, receiver and transmitter antenna gains as well as a somewhat complex geometry that involves the angle of the meteor trajectory with respect to the plane containing the transmitter, meteor trail and receiver, and other factors such as the ionosphere's variability especially at HF. Readers interested in additional technical detail should refer to [McKinley] or [Sugar], both of which present analyses for both forward and back scatter situations.

A Doppler frequency shift often is observed in the received signal caused by the motion of the meteor trails. Although meteors are moving at a constant linear velocity that is quite high, on the order of tens of  $\text{km s}^{-1}$ , the Doppler shift of the received frequency is determined by the apparent radial velocity of the trail itself with respect to both the transmitter and receiver. The Doppler frequency is given by

$$\Delta f_d \approx f_{Tx} \cdot \left( \frac{\pm V_{MTx} \pm V_{MRx}}{c} \right) \quad (3)$$

where

$\Delta f_d$  Doppler frequency, difference between the transmitted and received frequencies (Hz)

$f_{Tx}$  Transmitter frequency (Hz)

$c$  Speed of light ( $\sim 2.998 \cdot 10^8 \text{ m s}^{-1}$ )

$V_{MTx}$  Meteor trail radial velocity with respect to the transmitter ( $\text{m s}^{-1}$ ), + when the trail is moving toward the transmitter, – when the trail is moving away from the transmitter

$V_{MRx}$  Meteor trail radial velocity with respect to the receiver ( $\text{m s}^{-1}$ ), + when the trail is moving toward the receiver, – when the trail is moving away from the receiver

Equation (3) may be rearranged to find the combined relative velocity,  $V_{Comb}$ , as in

$$V_{Comb} = (\pm V_{MTx} \pm V_{MRx}) \approx \frac{\Delta f_d \cdot c}{f_{Tx}} \quad (4)$$

It is not possible to determine the individual radial velocities with respect to the transmitter ( $V_{MTx}$ ) or receiver ( $V_{MRx}$ ) without more information, which is not available from the types of observations discussed here.

### 3. Considerations for Observations at HF

Propagation: The transmitted signals must have a usable path from the signal origination point to the meteor trail and from the meteor trail to the receiver. As mentioned in the previous section, because of the distances between the transmitters and receiver, the signals are assumed to originate from virtual transmitters. Examples of 1, 2, 3 and 4 hop paths are illustrated in figure 5.

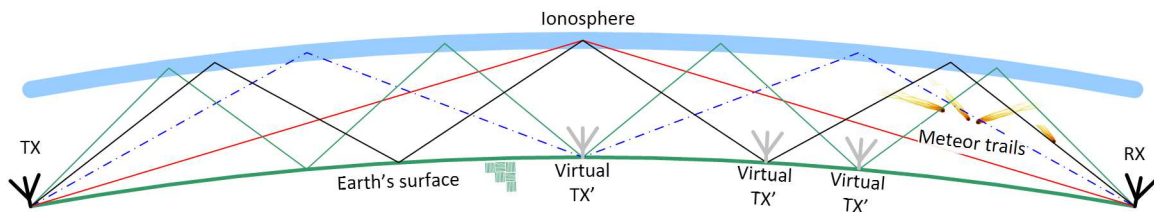


Figure 5 ~ Ground reflection points for 1-, 2-, 3- and 4-hop propagation paths from the transmitter (TX) to receiver (RX). Some example locations for virtual transmitters (TX') are shown at ground reflection points, all within about 2000 km from the receiver. The refraction points in the ionosphere also could be locations of virtual transmitters but they are not labeled here.

Examination of the path's geometric characteristics for various ionosphere reflection heights (table 1) indicates that 1-hop paths are highly unlikely except under exceptional propagation conditions. The 2-hop paths place a virtual transmitter at about 2000 km (WWV) and 2300 km (WWVH) from the receiver at Anchorage. These ranges are at the extreme limits for reception of meteor trail reflections for meteor heights near 90 km. The 3- and 4-hop situations are more likely because they involve distances of about 1100 to 1600 km from a virtual transmitter. Higher mode paths are possible. However, during daylight hours, the transmitted radio waves pass through the D-region twice on each hop's and the repeated absorption on high-mode paths could significantly weaken the signal before it gets to a virtual transmitter point. For propagation at night, the D-region all but disappears and probably is not an impairment.

To support propagation in the 15 to 25 MHz range, the ionosphere's F-region between the transmitters and receivers must be developed enough to refract the radio waves. The upper ionosphere along the paths starts developing around sunrise at WWV (longitude 105° west) but before sunrise at Anchorage (longitude 150° west). The situation is different for WWVH (longitude 159° west) with sunrise occurring about the same time at both stations. As discussed below, the best time to observe meteor trail reflections is in the morning when the receiver is on the side of Earth facing in the direction of Earth's orbit. It turns out that for my observations the ionosphere develops around the right time in the morning for both propagation and meteor reflection.

Daily, seasonal, yearly and long-term variations: Scientific observations over the years show that the rates at which meteor trail reflections are observed significantly varies throughout the day, seasons, solar cycle and Earth's position in its orbit around the Sun. In terms of daily (diurnal) variations, the meteor rate depends somewhat on the local time, with times around local sunrise (about 6:00 AM) having the highest rate and

around sunset (about 6:00 PM) the lowest rate. This is due to the rate at which meteors are captured by Earth's gravity and intercepted by its atmosphere as it rotates (figure 6). The Sun transits Anchorage around 2200 UTC (with slight variations at different times of the year), so the station directly faces Earth's orbital path 6 h earlier at 1600 UTC. This would be the approximate peak time; meteors could be swept up for a few hours before and after.

Table 1 ~ Propagation path geometric characteristics between transmitters at WWV and WWVH and receiver at Anchorage for F-region ionosphere heights  $H = 250, 300$  and  $350$  km. Distances per hop segment are straight line distances in km. Hop angles are elevations above the horizon in  $^\circ$ . The calculations assume an earth radius of 6370 km, equal distances between ground reflections and ionosphere refractions and that projection of the propagation paths on the ground follow great circle paths (no off-path reflections or refractions). For multi-hop paths, it is assumed that the refraction heights are identical on all hops. Note: For the cases indicated by \*, the minimum height required for 1-hop refraction is 308 km on the WWV path and 386 km on the WWVH path. All distance and angle calculations are according to {Reeve-IDC}.

H = 250 km	Great Circle	1-hop	Segment	2-hop	Segment	3-hop	Segment	4-hop	Segment
Path	Distance	Angle	distance	Angle	distance	Angle	distance	Angle	distance
WWV → ANC	3801	< 0	*	10.2	1000	18.3	692	25.1	545
WWVH → ANC	4414	< 0	*	7.5	1151	15.1	790	21.5	615
<b>H = 300 km</b>									
WWV → ANC	3801	< 0	*	12.8	1017	22.0	714	29.5	571
WWVH → ANC	4414	< 0	*	9.9	1167	18.4	810	25.5	639
<b>H = 350 km</b>									
WWV → ANC	3801	1.5	1976	15.4	1036	25.4	739	33.5	600
WWVH → ANC	4414	< 0	*	12.1	1185	21.5	832	29.2	666

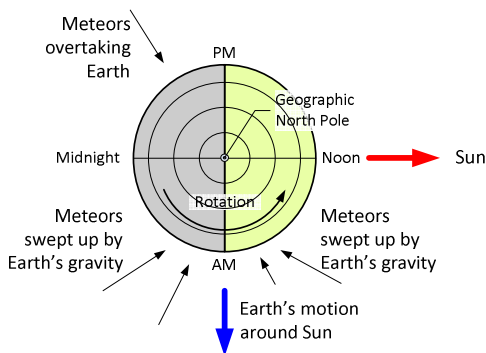


Figure 6 ~ View of Earth from above the North Pole. Daily variations in meteor trail detections at any given location are caused by the higher rate of capture and interception of meteors in the morning hours (AM) as Earth moves through its orbit around the Sun and intercepts the dust and debris trails left by comets and asteroids. Earth's speed in the direction of its orbit is about  $30 \text{ km s}^{-1}$ . The only meteors reaching Earth during the evening hours (PM) are those with a speed high enough to overtake it.

Seasonal variations in meteor activity are due to the tilt of Earth's rotation axis with respect to its orbital plane (ecliptic plane). The northern hemisphere's tilt in the direction of its orbit peaks in September (near the fall equinox), and its frontal area is maximum during that time period (figure 7). The opposite is true in late March (spring equinox). In the case of long distances between the transmitter and receiver, which is the case for the WWV and WWVH to Anchorage paths, seasonal variations in HF radio propagation also exist. The Sun controls Earth's ionosphere and significantly influences HF radio propagation, so the solar cycle also will affect detection of meteor trails.

The rate at which meteor trail reflections are detected increases during meteor *showers*, many of which occur annually as Earth intercepts the dust and debris shed by comets and asteroids during their long orbits around the Sun. Over 900 suspected and 100 well established meteor showers are listed by the Meteor Data Center of

the International Astronomical Union at [{MDCIAU}](#). Meteor showers are characterized by their *radiant* and *zenith hourly rate* (ZHR). The radiant is the point in the sky from which the meteors in a shower appear to originate. The ZHR is the estimated number of meteors seen by an observer during a 1-h period with the shower's radiant directly overhead (zenith).

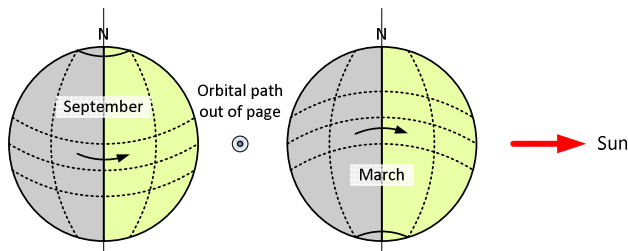


Figure 7 ~ Views of Earth from the perspective of a meteor aligned with Earth's orbital path during September and March. The seasonal variations at a given location are caused by the tilt of Earth's rotation axis. The northern hemisphere has more frontal area and sweeps up more meteors in the fall.

There also are many, many *sporadic* meteors that are not associated with any shower. The preponderance of meteor mass entering Earth's atmosphere is sporadic. The shower and sporadic meteors are not evenly distributed throughout any given year, resulting in a maximum in July and a minimum in February by a ratio of 2:1 to 6:1 depending on how they are reported.

Spectra: Meteor trail reflections very often are recorded on spectrograms, and interpreting the spectrograms is an important part of the observations. For example, it is possible to misinterpret aircraft reflections as meteor trail reflections. Meteor trail reflections may involve Doppler frequency shifts. The change in frequency due to Doppler effects is related to the radial speed of the object with respect to both the receiver and transmitter. These radial speeds may be much less than the speeds of the meteors along their trajectory. Thus, the spectra of reflections from meteor trails may show a range of frequency shifts.

Although the meteor trail is considered to be a long thin trail of electrons, high altitude winds with both horizontal and vertical shear and fragmentation of the meteor lead to spectra signatures that show striations, spreading and diffusion. The durations of meteor trail reflections are quite variable, from fractions of a second to many minutes. Short duration meteor trail reflections at HF display as a blip or tick on the spectra while long duration reflections are more stretched out and often striated; some reflections show both characteristics.

In the case of the Anchorage observatory, a spurious carrier sometimes can be seen drifting through the spectra. Spectra signatures possibly caused by signal processing artifacts including aliasing are hard to interpret and may exist in some of the records. Receiver artifacts have been ruled out by running the receivers for long time periods while connected directly to an RF signal generator and noting no effects whatsoever.

---

#### 4. Instrumentation

The instrumentation originally was setup during summer 2014 and has operated almost continuously since then with some hardware updates along the way. All observations are taken in the HF band using the WWV and WWVH time-frequency transmitters as the signal sources.

A block diagram of the receiver and antenna system at Anchorage shows the station setup (figure 8). Because of the equipment integration and multi-use configuration of the Anchorage station, equipment may be temporarily repurposed for a different project.

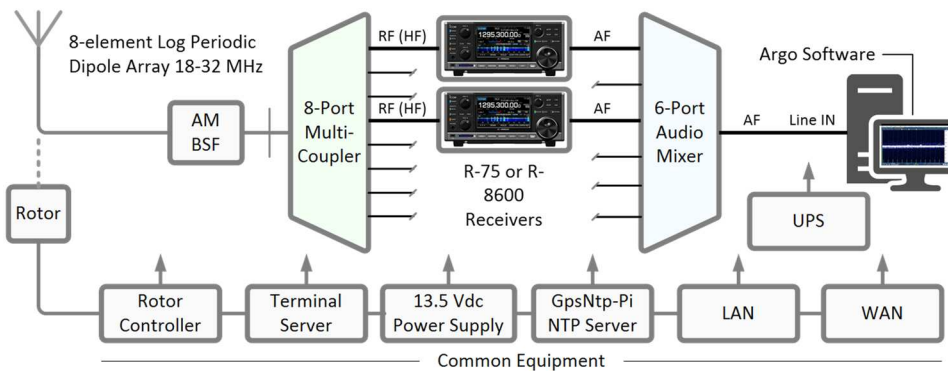


Figure 8 ~ Receiver and antenna system block diagram. PC timing is controlled by two GPS receiver-based network time protocol servers. Common equipment includes infrastructure shared with other observatory equipment. The antenna usually was rotated to point at WWV on a true bearing of 107°.

The receivers generally are tuned to fixed frequencies for long time periods, specifically, the WWV and WWVH transmitters at 15 and 20 MHz and WWV at 25 MHz. Over the years of observation, the frequency during any given time period usually was based on the best daytime reception, which changed over time. Most observations in 2020 were made with only one R-75 receiver, and it usually was tuned to 15 MHz. However, in late 2020 I installed two R-8600 receivers. The new receivers were tuned to 15 and 25 MHz. The R-75 receivers are equipped with the optional CR-282 high-stability crystal, which significantly reduces oscillator drift and stabilizes the signal trace on the Argo display. The R-8600 receivers are factory-equipped with high-stability oscillators.

The demodulated audio output from each receiver is fed through an analog stereo audio mixer and then to the PC soundcard Line In jack. The audio mixer allows up to six receivers to share one soundcard input and can be configured for any receiver output on any channel input. I usually operate the receivers in lower sideband (LSB) mode with the AGC turned off, and I usually tune one receiver 1000 Hz and the other 990 or 1010 Hz above the carrier frequency so that they display distinctly different traces in Argo. The offset tuning with LSB provides a nominal 1 kHz beat note, and it is this beat note that is processed by the Argo software, not the carrier itself. I usually operate the receivers with their RF gain set to maximum and their internal preamplifier or attenuator turned off. These settings may be changed when the receivers are temporarily used for other projects but always restored for long-term operation.

The antenna is an 8-element log periodic dipole array (LPDA) with a design frequency range of 18 to 32 MHz and mounted 13 m above ground level with an elevation angle of 0°. The antenna may be rotated to any azimuth but for most observations in 2020, the antennas was pointed 107° True toward the WWV station. The horizontal beamwidth is on the order of 60°, and the vertical beamwidth has several lobes from 10° to 30° and 60° elevation. No attempt was made to determine if different antenna directions change the meteor echo detection rate.

The Argo software is setup to display a horizontal waterfall that shows a narrowband representation of the demodulated received carrier over time, thus allowing small frequency shifts and deviations to be observed and recorded (figure 9).

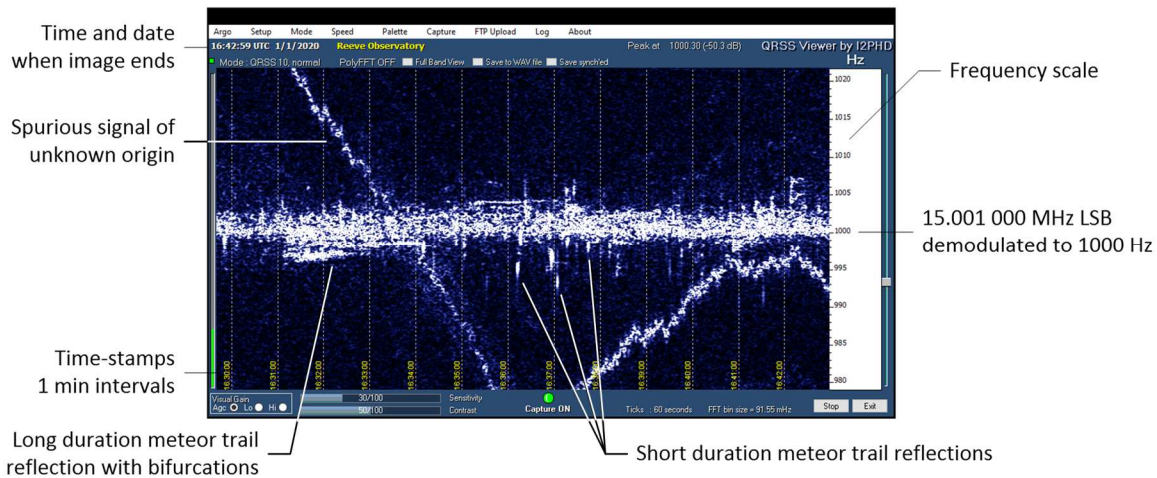


Figure 9 ~ Annotated Argo image pointing out the time-stamps, frequency scale and ending time and date for the plot. The plots typically have a 12 min time span. This example from 1 January 2020 also shows numerous short duration meteor trail reflections and at least one long-duration reflection. Sometimes spurious signals of unknown origin drift through the spectrum but they are easily recognized and usually do not obscure spectra of interest.

The Argo software originally was developed for displaying very low speed, weak signal, digital communication modes but is used here to display the demodulated WWV or WWVH carriers in a nominal  $1000 \pm 20$  Hz frequency span. The span is determined by the mode, in this case QRSS10 (derived from the radiotelegraph Q-code *QRS* and a CW dot length of 10 s). A list of settings is provided below (table 2).

Table 2 ~ Argo software settings

Menu	Settings
Setup	Autorun when program starts, 0 dB = ADC Full Scale
Mode	QRSS10, Long ticks, Show seconds in ticks, Auto ticks interval
Capture	720 s
Speed	Normal
Palette	Standard
FTP upload	Auto enable upload at program start, Upload enabled

Argo not is capable of recording the FFTs produced by its processing, so all analyses are based on periodic screenshots of the spectra that were automatically recorded as Portable Network Graphics (.png) files. An image is recorded every 12 minutes, corresponding to the displayed time span, and then saved with a sequence number or time-stamp to an archive. The image dimensions are 1000 x 597 pixels. The images also are sent to my website and displayed in near real-time. Image file sizes vary from around 20 kB to 200 kB depending on the displayed activity. The software runs continuously, producing 120 image files per day.

## 5. Observations of Meteor Trail Reflections

The Argo images shown in this section were taken from my 2020 files, and represent only a small sample of the images that show meteor trail reflections. A total of the almost 42 600 images from 2020 were viewed. A summary is given below (table 3) followed by discussion and the Argo images in chronological order. If

necessary, refer to figure 9 for a description of the information shown on the Argo images. it should be remembered that the traces shown on the Argo images include both the demodulated spectra of the signal reflected by meteors and the demodulated spectra of the signal that is received as the result of ionospheric propagation and has not been reflected by meteors.

Table 3 ~ Summary of Argo images shown in this section

Note: Time (solar) = Time (UTC) – 10 h.

Figure	Date (UTC)	Time (UTC)	Time (Solar)	Image length	Freq. (MHz)	Shower
10	1 Jan 2020	1830 – 1842	0830 – 0842	12 min, single	15	Quadrantids
11	2 Jan 2020	1618 – 1642	0618 – 0642	24 min, splice	15	Quadrantids
12	3 Jan 2020	1718 – 1742	0718 – 0742	24 min, stich	15	Quadrantids
13	6 Jan 2020	1630 – 1642	0630 – 0642	12 min, single	15	Quadrantids
14.a	6 Jan 2020	1718 – 1855	0718 – 0855	96 min, splice	15	Quadrantids
14.b	6 Jan 2020	1730 – 1742	0730 – 0742	12 min, single	15	Quadrantids
15	12 Jan 2020	1730 – 1742	0730 – 0742	12 min, single	15	Quadrantids
16	13 Jan 2020	2106 – 2130	1106 – 1130	24 min, splice	15	Capricornids
17	14 Jan 2020	1757 – 1812	0757 – 0812	15 min, splice	15	Capricornids
18	28 Jan 2020	1742 – 1754	0742 – 0754	12 min, single	15	Capricornids
19	29 Jan 2020	1706 – 1718	0706 – 0718	12 min, single	15	Capricornids
20	1 Feb 2020	1543 – 1655	0543 – 0655	72 min, splice	15	Capricornids
21	18 Feb 2020	0056 – 0104	1406 – 1504	12 min, single	15	Unknown
22	04 Apr 2020	1733 – 1745	0733 – 0745	12 min, single	15	Unknown
23	06 Aug 2020	1724 – 1736	0724 – 0736	12 min, single	15	Perseids
24	19 Sep 2020	1530 – 1542	0530 – 0542	12 min, single	15	Sextantids
25.a	20 Sep 2020	1409 – 1555	0409 – 0555	106 min, splice	15	Sextantids
25.b	20 Sep 2020	1435 – 1448	0435 – 0448	12 min, single	15	Sextantids
26	21 Sep 2020	1422 – 1608	0422 – 0608	106 min, splice	15	Sextantids
27	04 Oct 2020	1421 – 1540	0421 – 0540	79 min, splice	15	Unknown
28	10 Oct 2020	0248 – 0300	1648 – 1700	12 min, single	15	Draconids
29	21 Dec 2020	1641 – 1653	0641 – 0653	12 min, single	15 & 25	Geminids

Audio: I often monitor the receiver audio but do not record the demodulated meteor echo signals. Generally, the signal bursts are very weak and short and it is impossible to know if any given reflection involves WWV or WWVH. The short-duration echoes sound like 1 s or less bursts of tone or tone enhancements. When there are continuous streams of short-duration echoes, they sound like low-speed CW demodulated at 1000 Hz. Short tone bursts with a Doppler frequency shift have a bell or multiple bells sound or they sound like a wind chime.

Long-duration echoes are distended. Long-duration echoes with striations usually have a wavering tone corresponding to a few to several Hz frequency difference; these bursts have a distinctly different tone. As propagation improves in the morning, the tone bursts meld into a steady tone, at which time I can discern the female voice announcements from WWVH and male voice from WWV, but the 1000 Hz offset and LSB mode make the announcements unintelligible (severe duck talk).

Detection times and rates: Most meteor trail reflections were detected between about 1400 and 1900 UTC, which corresponds to local solar times 4:00 am to 9:00 am. A few images show unusual traces that are thought to be meteor trail reflections but were detected outside the normal morning time frames. Most reflections were detected before sunrise at Anchorage. Reflection events were recognized in the records from all months but not every day. Because of other projects during May 2020, records for only a few days are available during that month. The month of June produced few records of activity while January and October 2020 produced many records. There were no obvious seasonal variations in the detection times.

The low detection rate during some months probably has more to do with propagation conditions than the meteors themselves. The records show that the number of detected echoes decreased as propagation improved with the morning development of the ionosphere (the 1 s marker tones and voice announcements from the time stations were easily heard), likely indicating that the propagation mode changed and the geometry became less favorable for meteor trail reflection. The favorable propagation window usually lasted less than 3 h.

Spectra and durations: I have broadly classified echoes as short-duration and long-duration. These probably correspond to underdense and overdense echoes, respectively. Short-duration echoes appear on the Argo waterfalls as vertical ticks or blips lasting perhaps a fraction to a few seconds (Argo does not have sufficient time resolution to accurately determine short-duration echo time spans). Long-duration echoes are displayed as horizontal features or stripes lasting longer than a fraction of a minute. Some events, such as long-duration echoes or sequences of many echoes, overlap two or more 12 min Argo images, so some images in this section have been spliced together to show the entire duration of the event. Some records show a continuous stream of short-duration echoes lasting almost a couple hours.

The vast majority of meteor trail reflections detected at Anchorage are short duration. A number of long duration reflections were recorded, some lasting 5 to 7 min. These are remarkably similar to the spectra shown and discussed in [Bourdillon]; in fact, it was that paper that convinced me my Argo images showed meteor trail reflections. With one exception, the Argo images in this section are at 15 MHz. One image recorded both 15 and 25 MHz and the 25 MHz trace is WWV (only WWV has a 25 MHz transmitter).

The live Argo spectrum display includes a mouse cursor function that shows the relative power level at the cursor location. As noted in section 4, Argo is setup so that 0 dB corresponds to full scale of the soundcard analog-digital converter (ADC). When I have examined individual echoes on a live display, their relative power levels generally are 10 to 20 dB above the background noise level.

Doppler frequency: The maximum frequency shifts seen in the spectra due to Doppler effects are on the order of  $\pm 5$  to  $\pm 10$  Hz, but there are a few exceptionally higher shifts. The corresponding Doppler velocities are 100 to 200  $\text{m s}^{-1}$ . Even though the meteor velocity itself is quite high, as discussed in section 2, it is the radial speeds of the ionized trail with respect to both the receiver and transmitter that determines the Doppler frequency shift recorded in the spectrograms. It should be noted that, because of the way Argo was setup, frequency shifts greater than  $\pm 20$  Hz are neither displayed nor recorded.

Some images, particularly spliced images of short-duration echo streams, clearly show that the Doppler shifts favor one polarity over the other. For example, the Doppler shifts seen in the 6 January 2020 record (figure 14.a) primarily are negative. The shift polarity may infer something about the direction of the meteor radiant or the direction of the meteors with respect to the transmitters and receiver, but I have not yet attempted to analyze that level of detail.

Striations: It will be noticed that most of the long-duration echoes shown below are striated. Some possible causes of the striations are: 1) Multiple trails produced by a group of associated meteors; 2) fragmentation of a meteor, which leaves more than one trail; 3) high-altitude wind shear that pulls the meteor ionized trail apart; or 4) interference between the reflected radio waves from different parts of the trail.

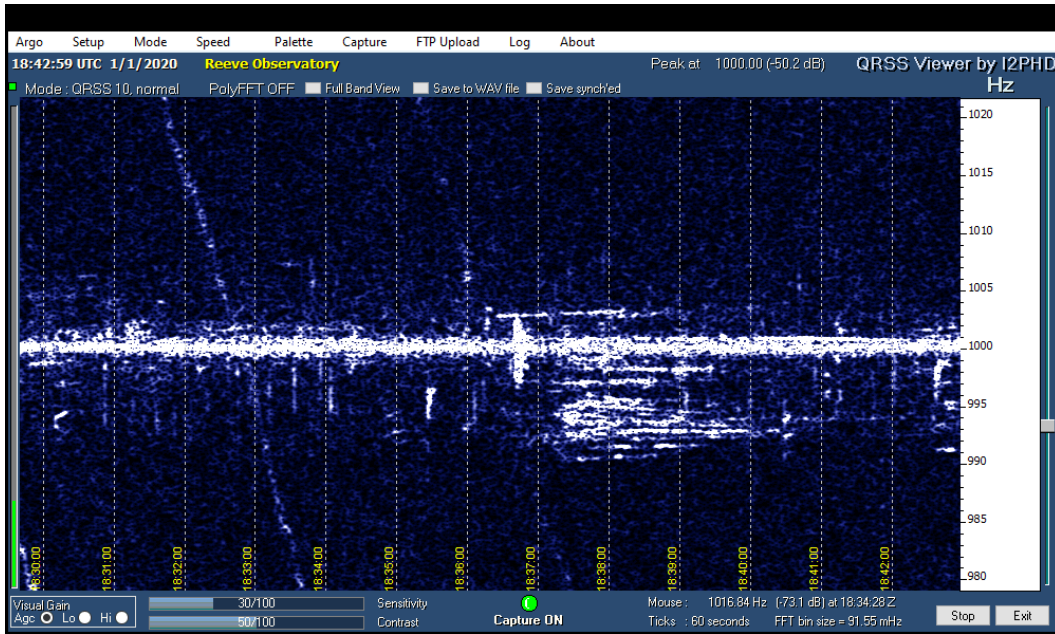


Figure 10 ~ Spectra showing multiple short-duration echoes between 1830 and 1842 on 1 January 2020 at 15 MHz. Several long-duration echoes also are visible starting about 1836:30, including three individual streaks and one striated echo. These all may be related. The slanted line at 1833 is a spurious signal drifting through the spectra.

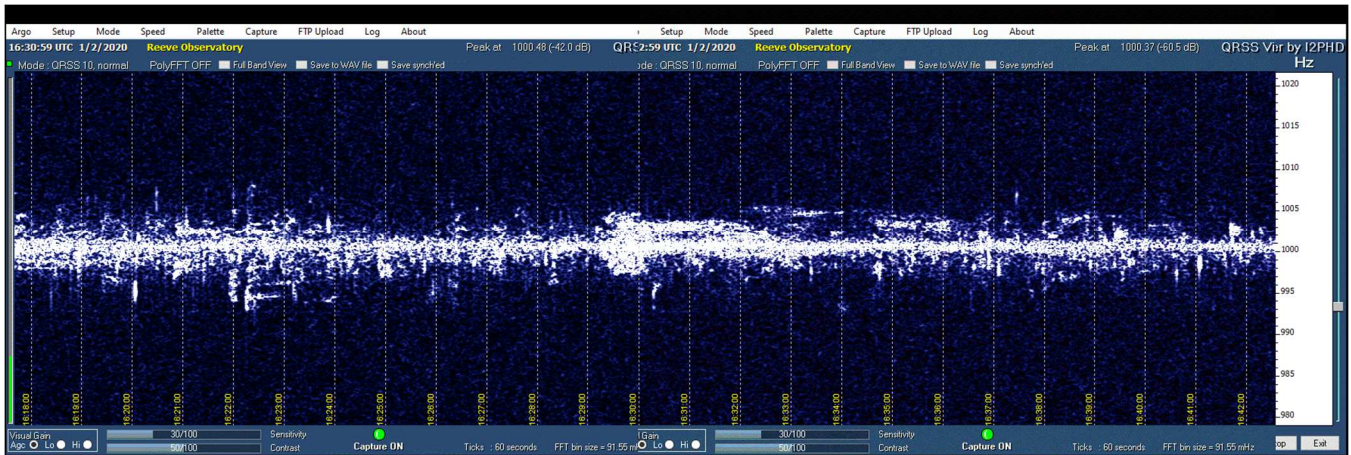


Figure 11 ~ Composite spectra of two 12-minute periods from 1618 to 1642 on 2 January 2020 at 15 MHz. Numerous short-duration echoes are apparent. A long-duration echo lasting about 4 min can be seen at 1630 (middle of image) with positive bifurcation. Many long-duration echoes detected at Anchorage show the bulbous beginning and striated tail as seen here. Others simply show striations as in the echo at 1622 in the middle of the left-half of this image.

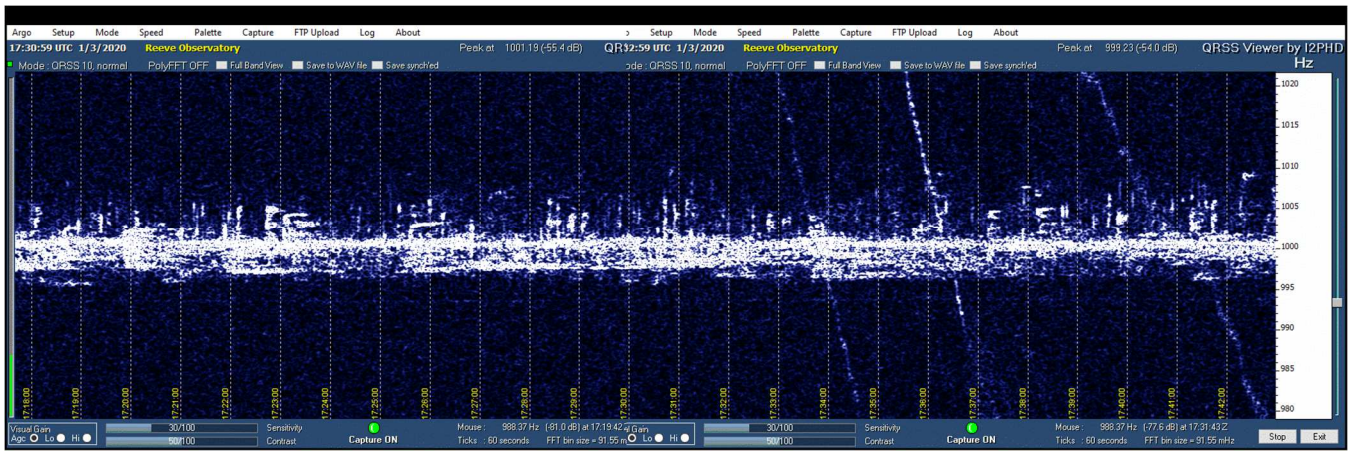


Figure 12 ~ Composite spectra covering two 12-minute periods from 1718 to 1742 on 3 January 2020 at 15 MHz. Numerous short-duration echoes are present with positive frequency shift. Several striated long-duration echoes also are visible, most with negative frequency shift. Spurious signals are marked by the three slanted lines in the right-half of the image, two of them very faint.

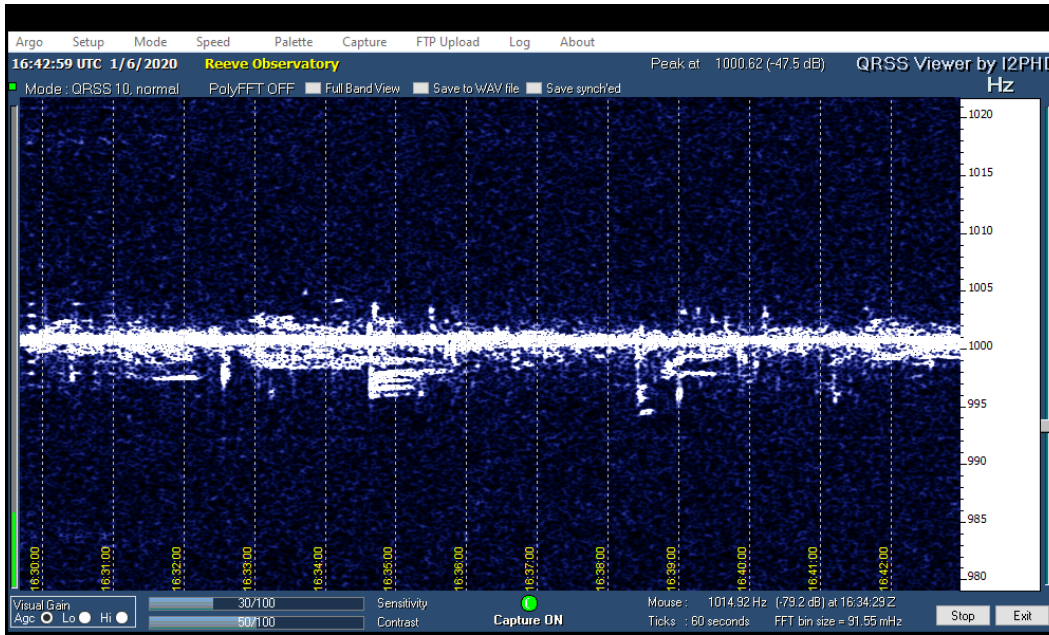


Figure 13 ~ Single 12-min image from 6 January 2020, 1630 to 1642 at 15 MHz. A long-duration echo with several negative striations is visible at 1635. Other long-duration echoes and several short-duration echoes also are visible.

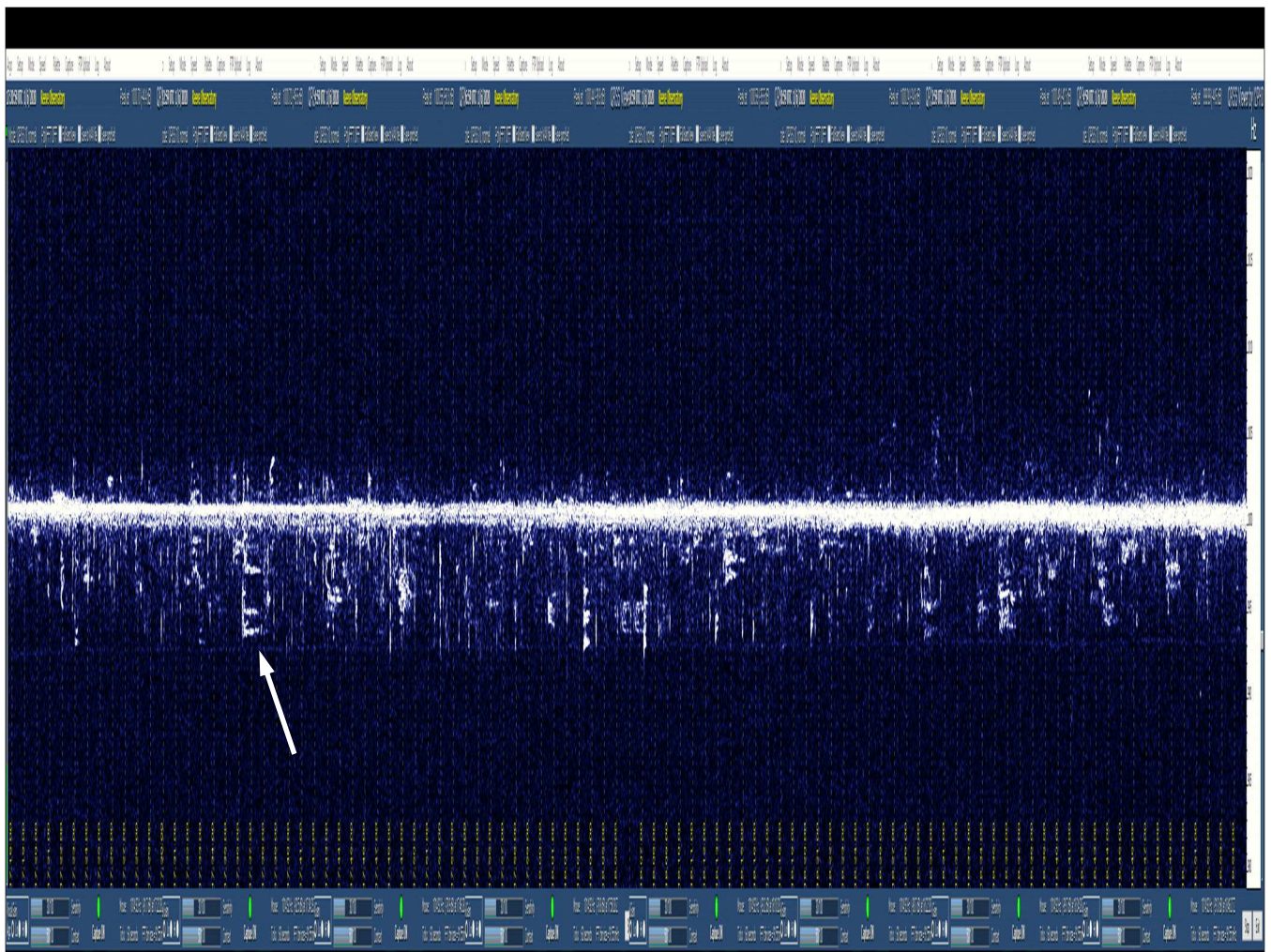


Figure 14.a ~ Eight spliced images from 6 January 2020 covering 1718 to 1855, 96 min total time span, showing continuous short-duration meteor trail reflections at 15 MHz. The spliced Argo image has been stretched vertically to emphasize the traces left by the short-duration reflections. Note that most of the reflections resulted in negative frequency shifts. The peak shifts are about  $-8$  Hz and are greater than the positive frequency shifts. Several striated long-duration reflections are visible, all with negative frequency shift. The arrow points to a feature for reference in the center of the next figure.

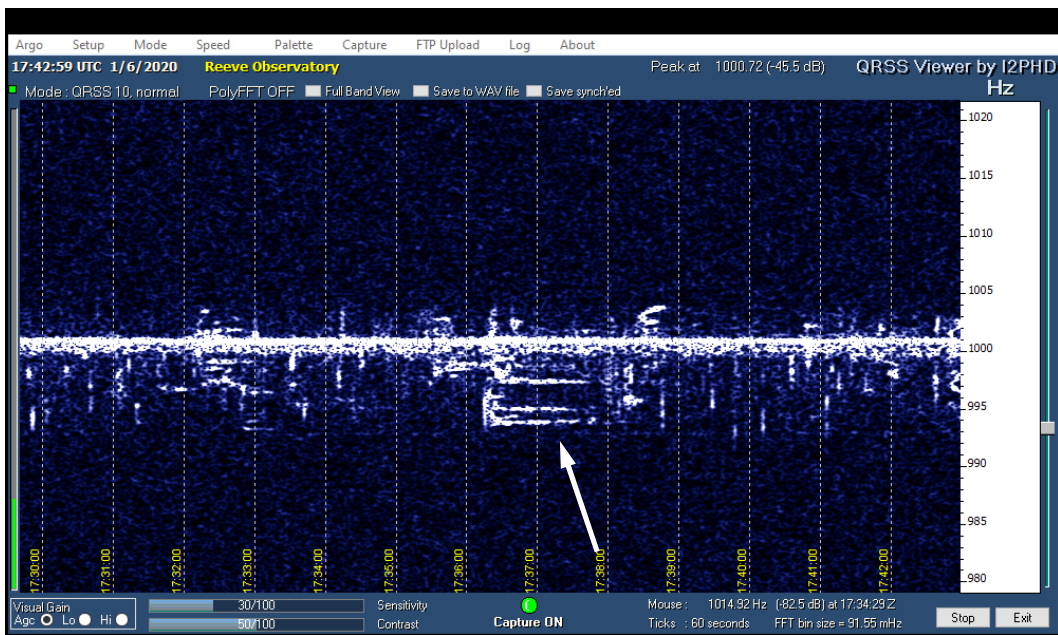


Figure 14.b ~ Image from 1730 to 1742 on 6 January 2020 at 15 MHz. This image is embedded in the composite spectra of the previous figure. The long-duration echo indicated by the arrow corresponds to the event pointed out by the arrow in the previous figure. There appears to be two long-duration echoes starting between 1736 and 1737, both with head echoes.

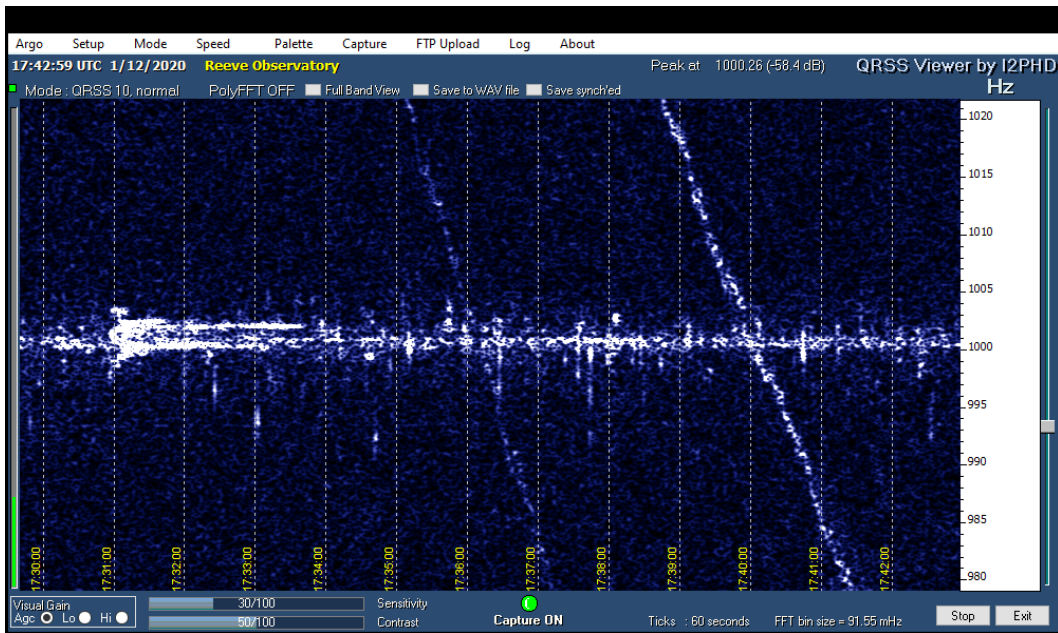


Figure 15 ~ Image covering 1730 to 1742 on 12 January 2020 at 15 MHz showing a long-duration echo starting at 1731 and lasting almost 3 min. This echo is bifurcated with slightly asymmetrical positive and negative frequency shifts. The curved head echo is discernible at the beginning. Many short-duration echoes also are visible. Two spurious signals have drifted through the spectra from high to low frequencies, the second stronger than the first.

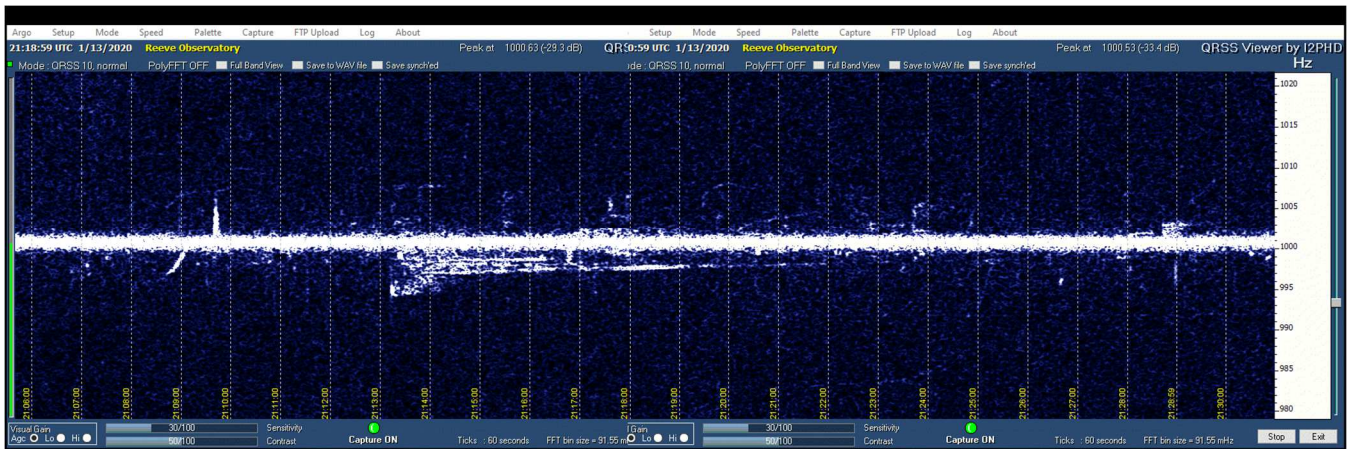


Figure 16 ~ Two spliced images from 2106 to 2130 on 13 January 2020 at 15 MHz showing another long-duration echo starting left of center just after 2113. Vestiges of this echo are visible until 2122, so the whole event lasted around 9 min. At least three striations, all with negative frequency shift, are visible. A strong short duration echo is seen about 3.5 min prior with positive frequency shift. The slanted, slightly curved trace below the centerline at 2109 probably is a light aircraft passing by the observatory at low altitude.

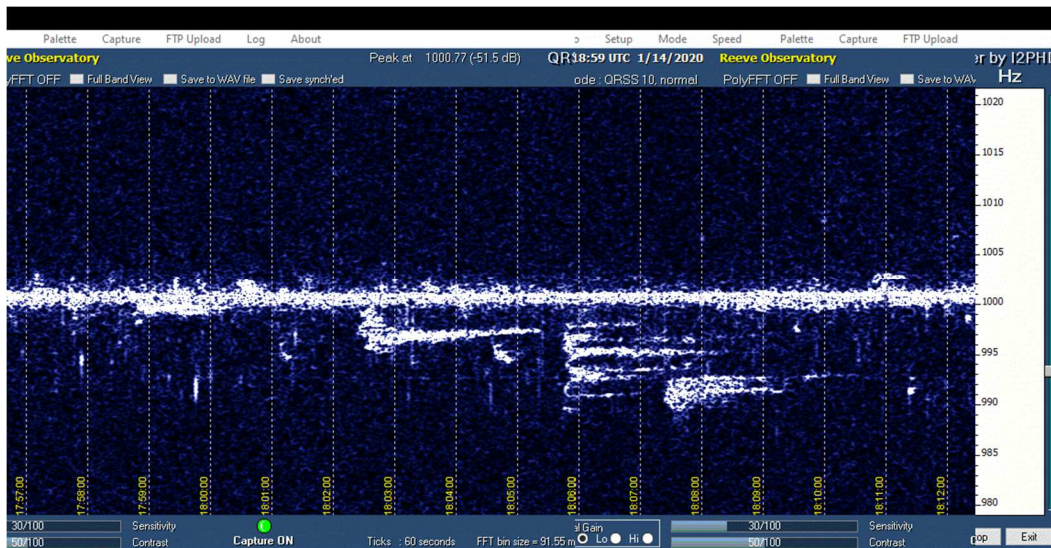


Figure 17 ~ Two spliced images from 1757 to 1812 on 14 January 2020 at 15 MHz showing at least three long-duration echoes and several short-duration echoes. The center long-duration echo starting around 1806 has at least seven striations. Almost all echoes in this record have negative frequency shift.

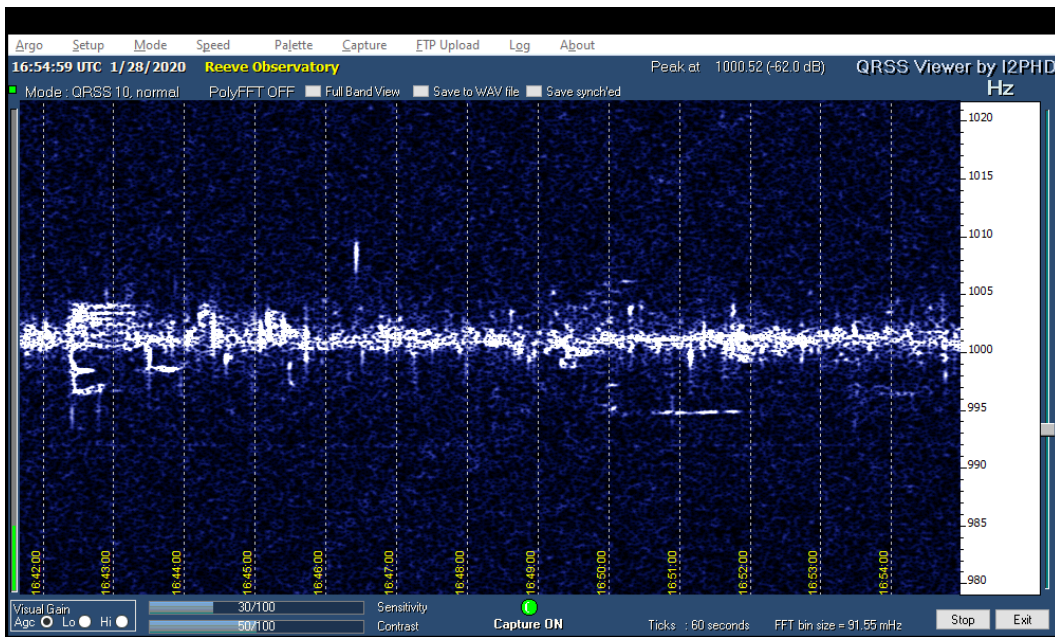


Figure 18 ~ The beginning of this image from 28 January 2020 for the time period 1642 to 1654 shows a long-duration echo with several striations at 15 MHz. It is not clear if the striations with positive frequency shift in this echo are related to those with negative shift. This image also shows numerous short-duration echoes including one between 1646 and 1647 with about 10 Hz positive frequency shift.

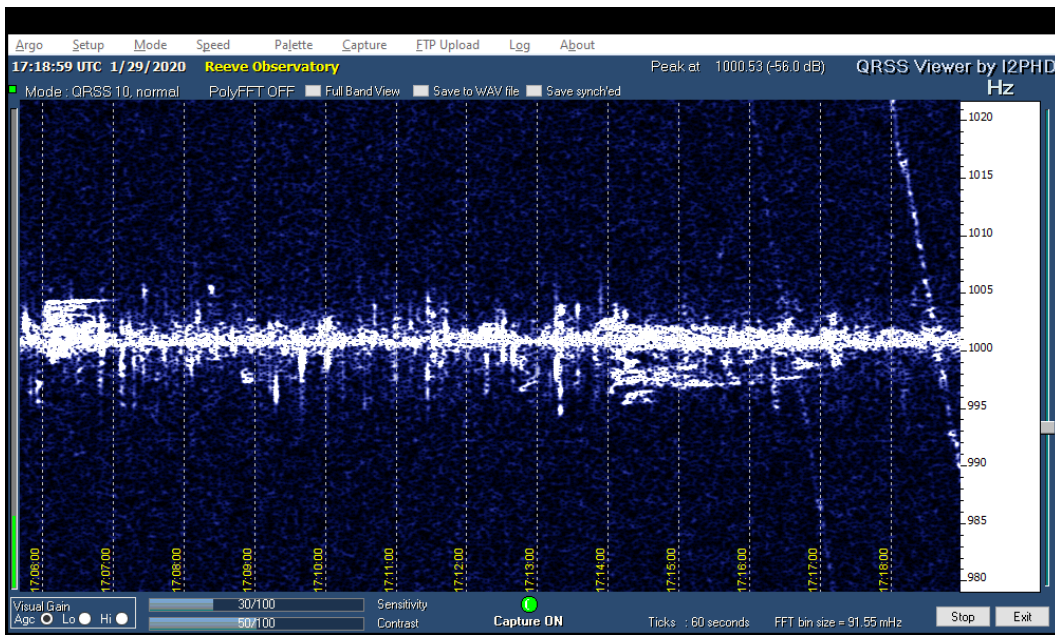


Figure 19 ~ Image from 29 January 2020 at 1706 to 1718 at 15 MHz shows a striated long-duration echo starting at 1706 and lasting 1 min. Many short-duration echoes are visible throughout the record along with another long-duration echo starting at 1714. A spurious signal drifted through at 1718.

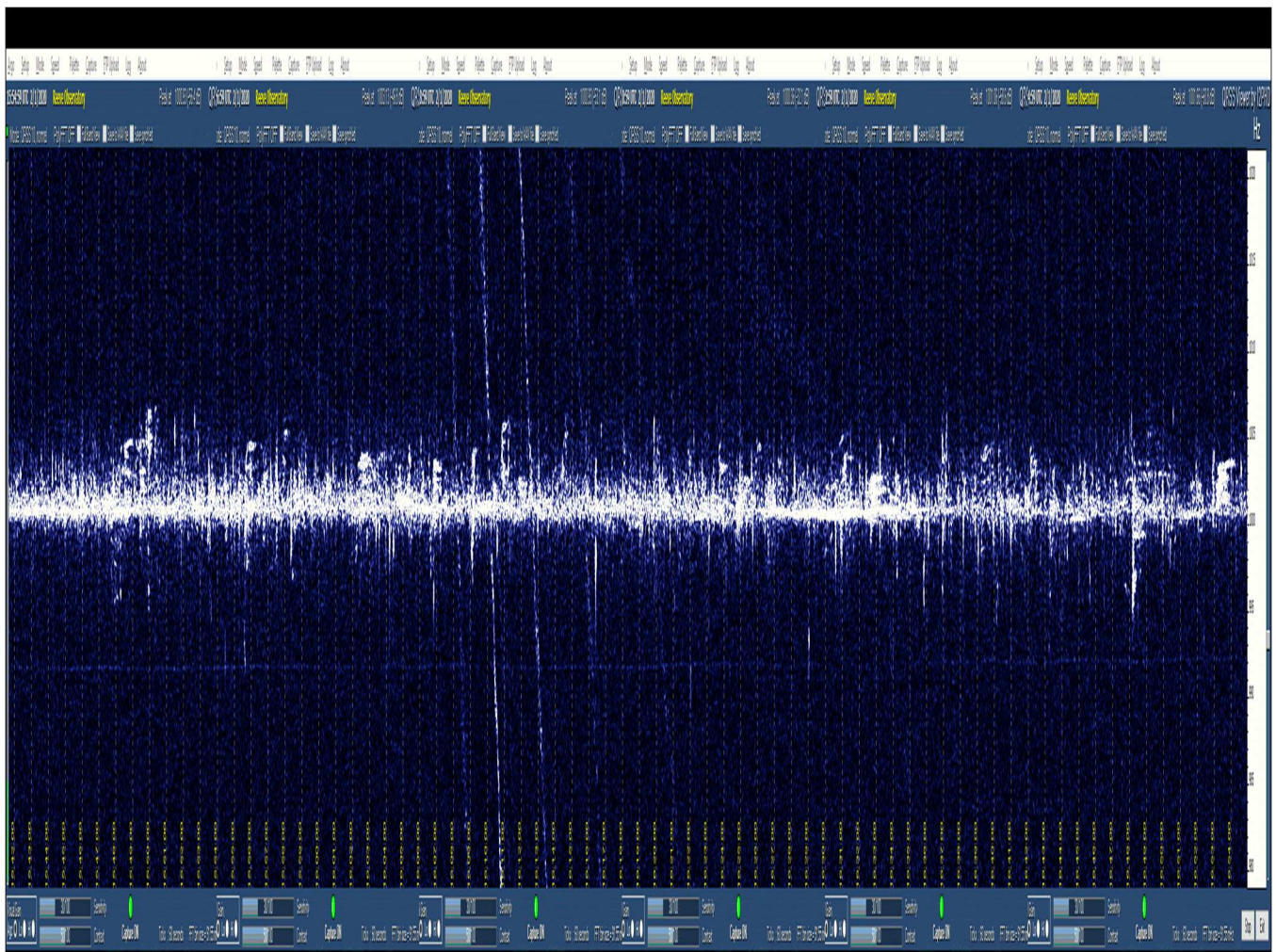


Figure 20 ~ Six spliced images from 1 February 2020 at 1543 to 1655, 73 min total duration showing a stream of short-duration meteor trail reflections at 15 MHz. Compare to figure 13.a. This spliced Argo image has been stretched vertically to emphasize the short-duration traces left by the reflections. Note that the reflections have a slight bias toward positive frequency shifts. The peak shift is about +6 Hz. A few striated long-duration reflections are visible, all with positive frequency shift. Two spurious signals drifted through the spectrum and are seen as steep slanted lines just left of middle covering the full 20 Hz frequency span of the waterfall.

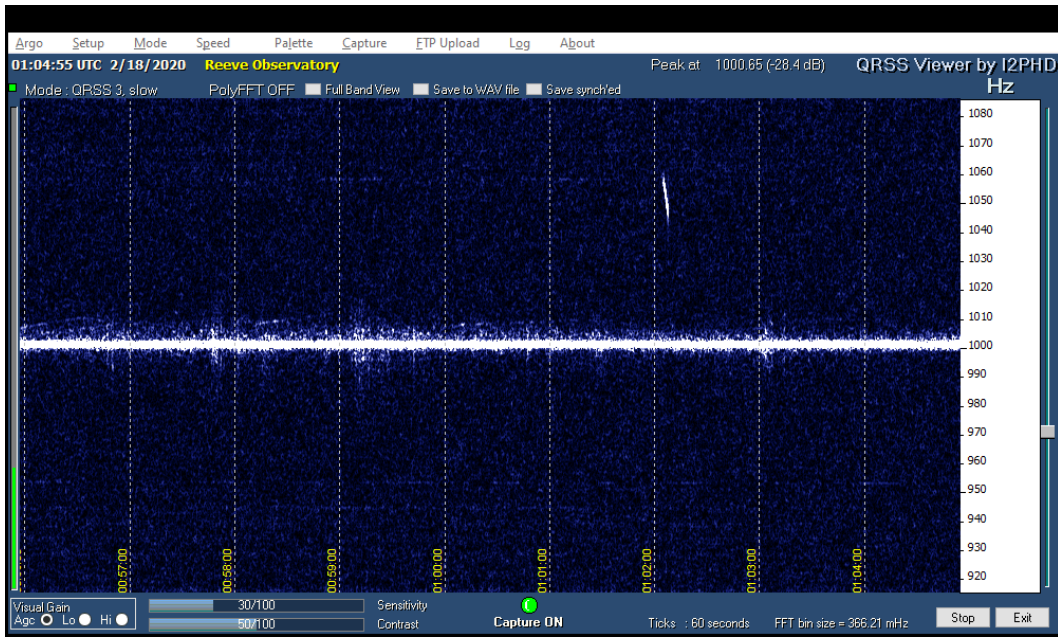


Figure 21 ~ Spectra from 18 February, 0056 to 0105 at 15 MHz. An isolated meteor trail reflection is visible just after 0102. Note that the frequency scale for this record was increased to  $1000 \pm 80$  Hz and that the echo has about 50 Hz positive frequency shift. This image includes what appears to be many short-duration echoes with much smaller frequency shifts.

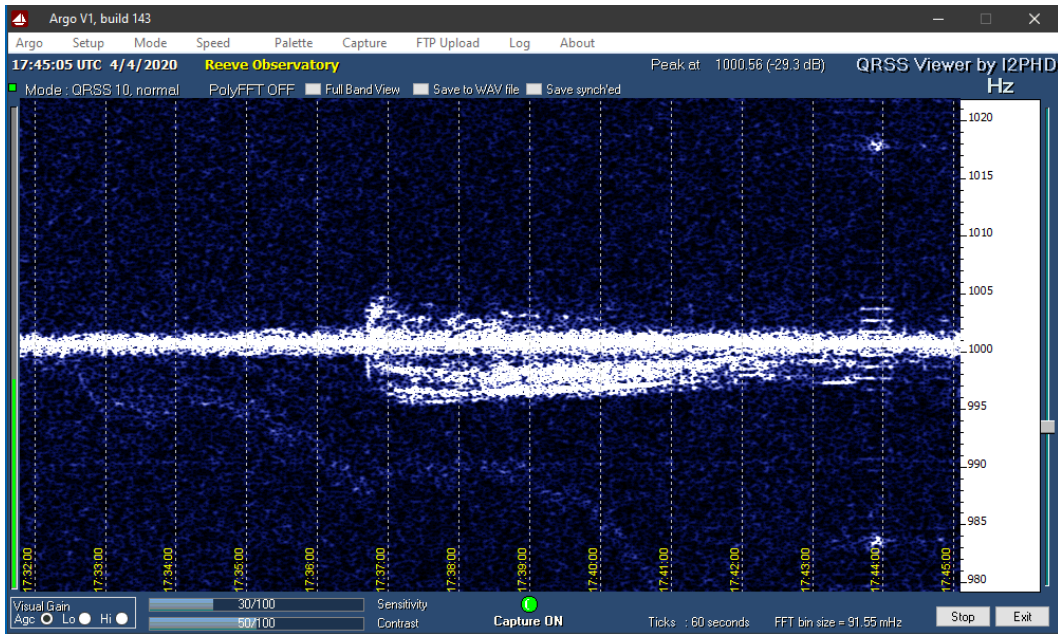


Figure 22 ~ Spectra from 4 April, 1732 to 1745 at 15 MHz. An isolated long-duration meteor trail reflection with a head echo is visible just before 1737 and includes several striations. This is one of the longer duration reflections from 2020, lasting about 7 min.

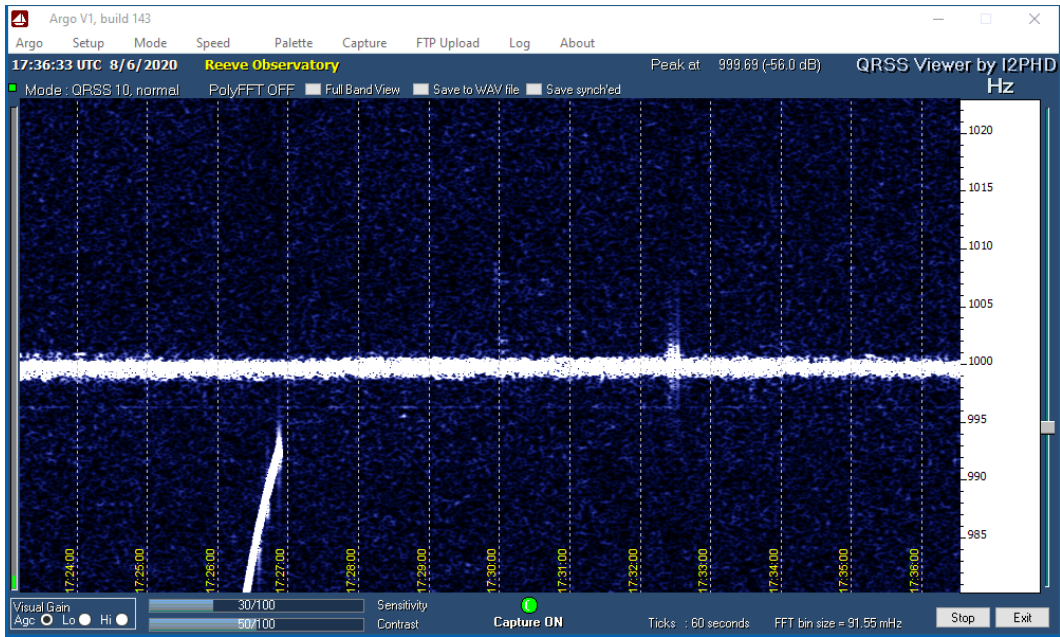


Figure 23 ~ Spectra from 6 August, 1724 to 1736 at 15 MHz. A trace, which may be a meteor trail reflection with relatively high frequency shift, enters the recorded spectra between 1726 and 1727.

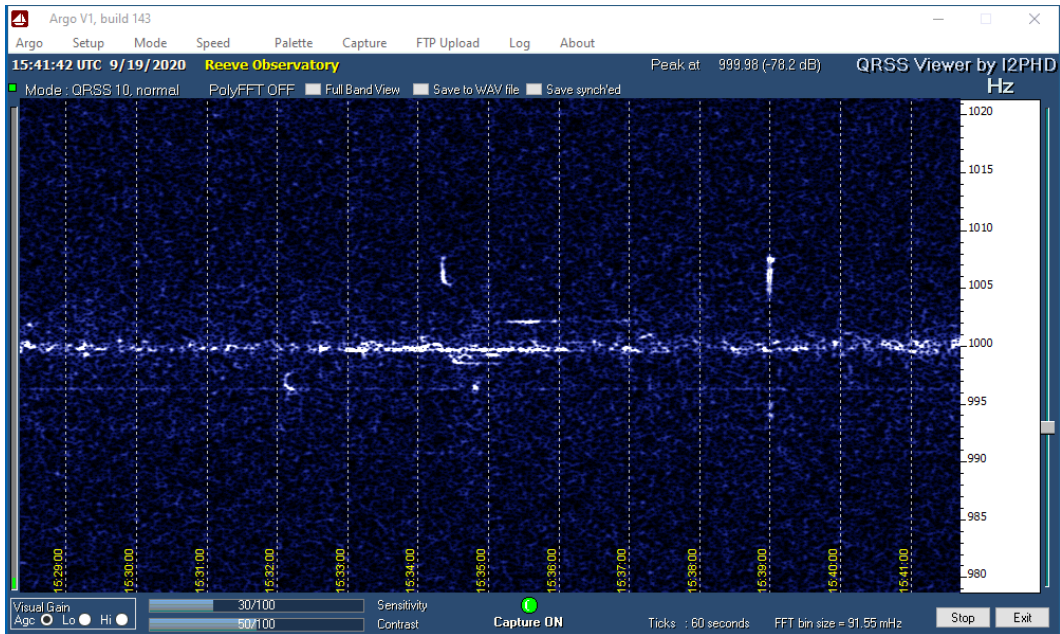


Figure 24 ~ Spectra from 19 September, 1529 to 1541 at 15 MHz. Two isolated short-duration echoes with positive frequency shift, one between 1534 and 1535 and another at 1539. Two or three echoes with negative shift also are visible.

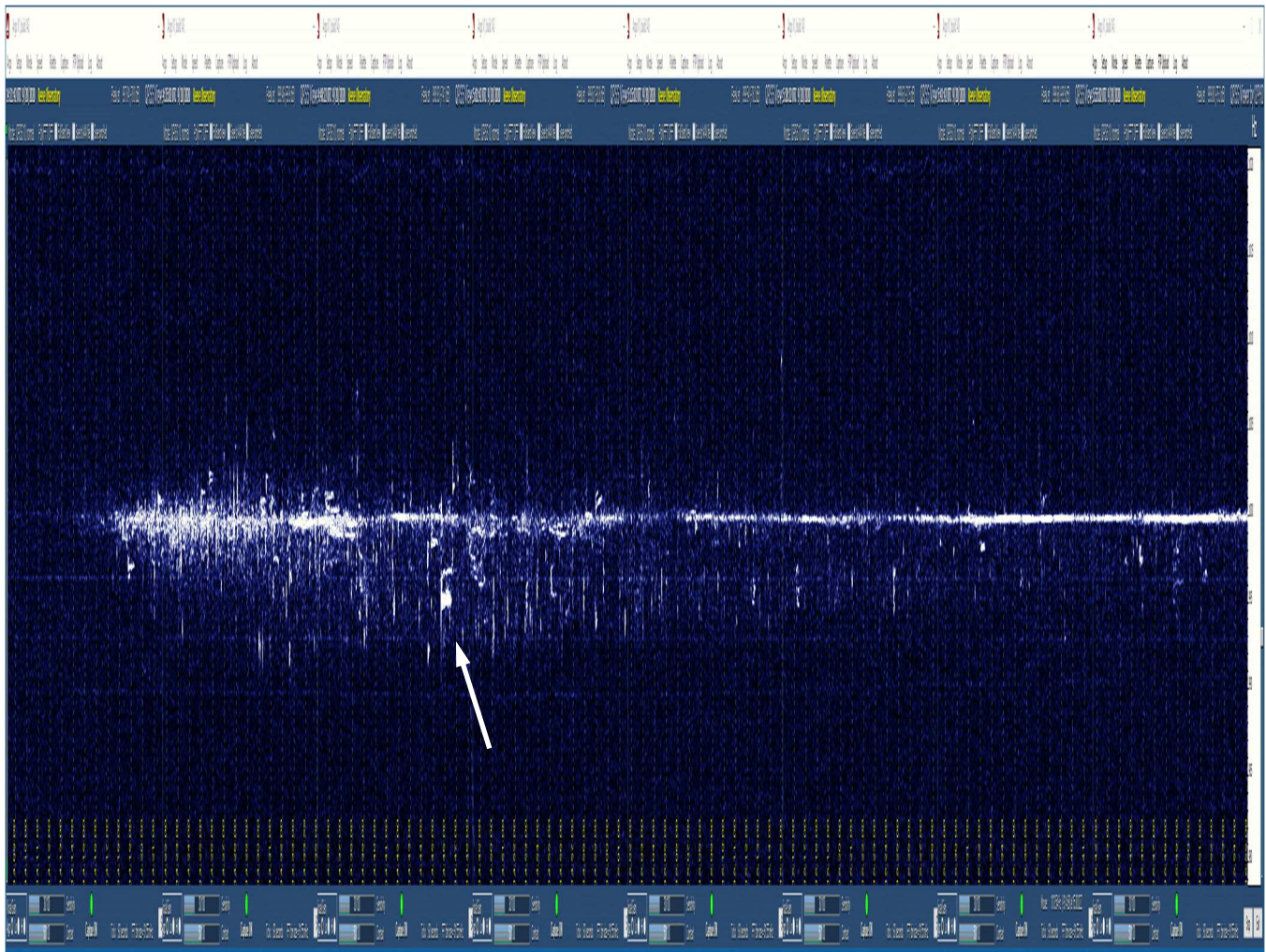


Figure 25.a ~ Eight images at 15 MHz for 20 September starting at 1409 and ending at 1555, spanning 106 min. The image has been stretched vertically to emphasize the echoes. The beginning of the record is blank because propagation was not supported by the ionosphere until about 1415. Very weak signals appeared at that time and a 1 min echo appeared at 1419. As propagation commenced, additional meteor trail reflections were detected, most with negative frequency shift. The stream of echoes was almost continuous until about half-way through the record to 1500 when they started to diminish. Although the number of echoes diminished after 1500, they still were present to the end of the record at 1555. The arrow is a reference point for the corresponding 12-min image shown in the next figure.

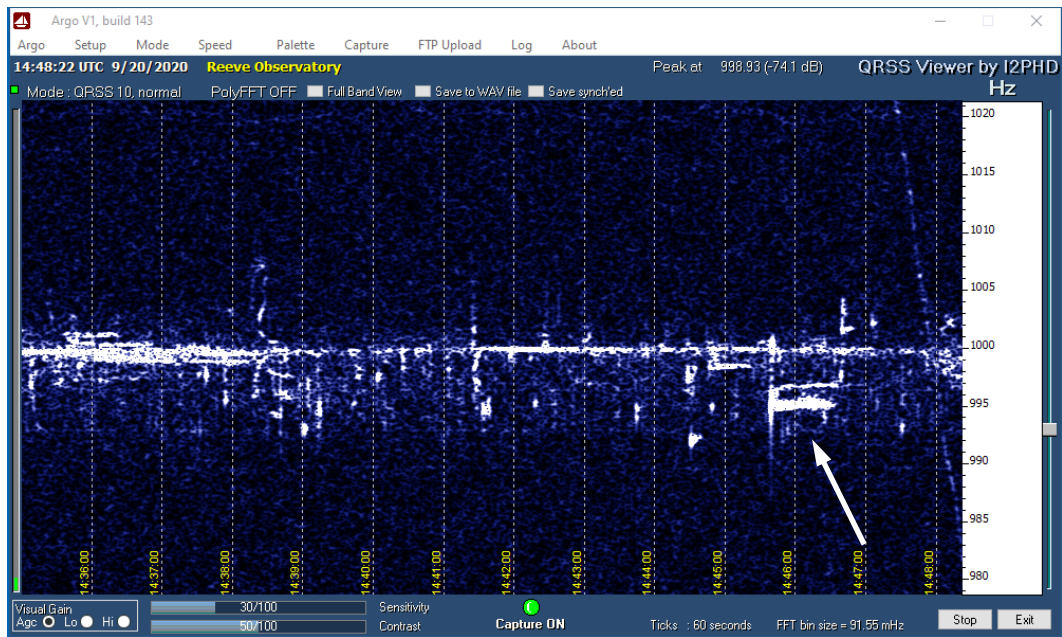


Figure 25.b ~ One of the eight 12-min images for 20 September embedded in the previous figure – this one is from 1435 to 1448 during the peak in the stream of short-duration echoes. The arrow points to a long-duration echo used as a reference point in the previous figure. This trace appears to show a head echo.

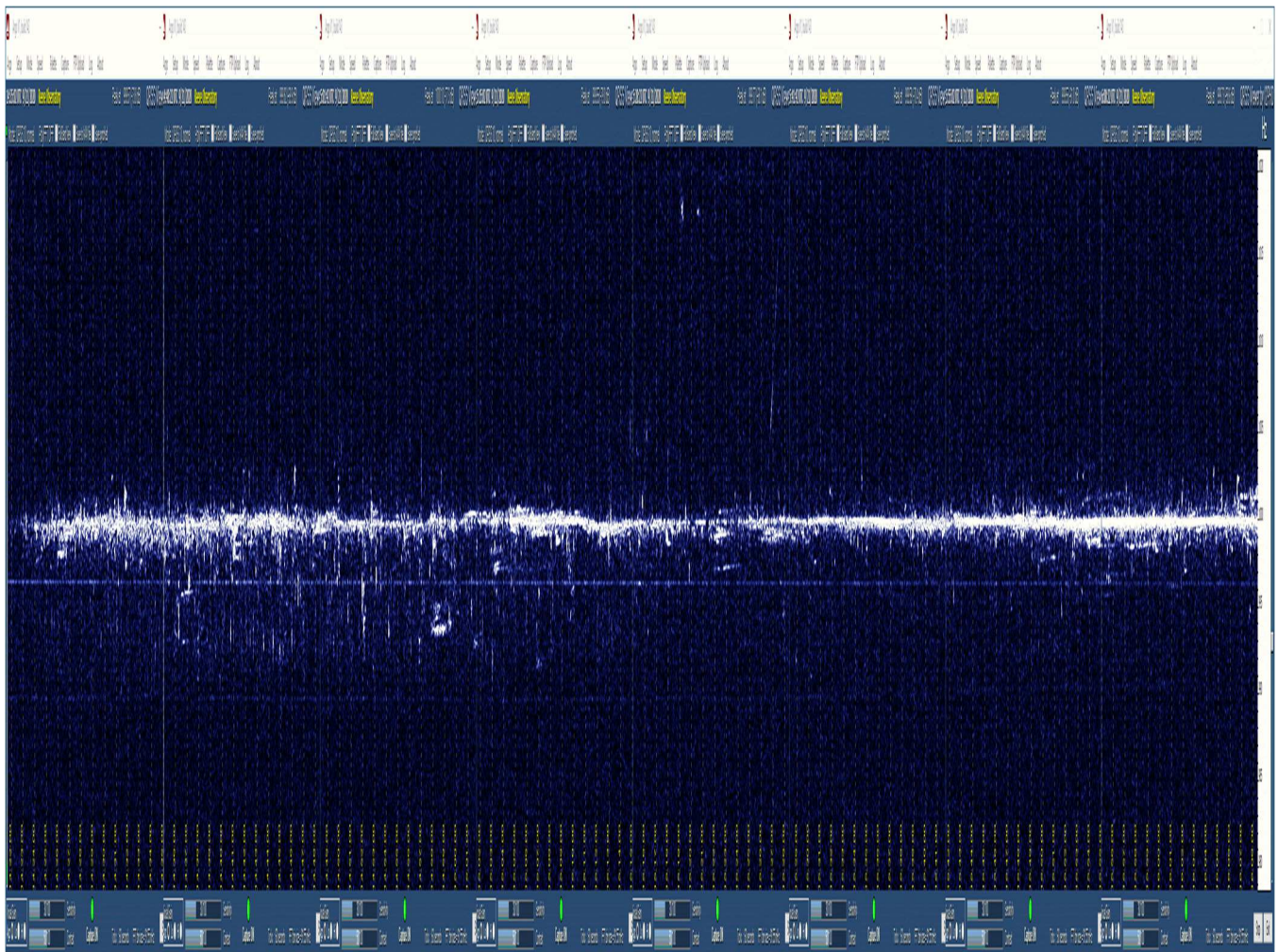


Figure 26 ~ Eight images at 15 MHz for 21 September starting at 1422 and ending at 1608, spanning 106 min and stretched vertically as in previous images. Compare to the spliced image in the previous figure from almost exactly 24 h earlier. The stream of meteor reflections continued for another 20 min until 1635.

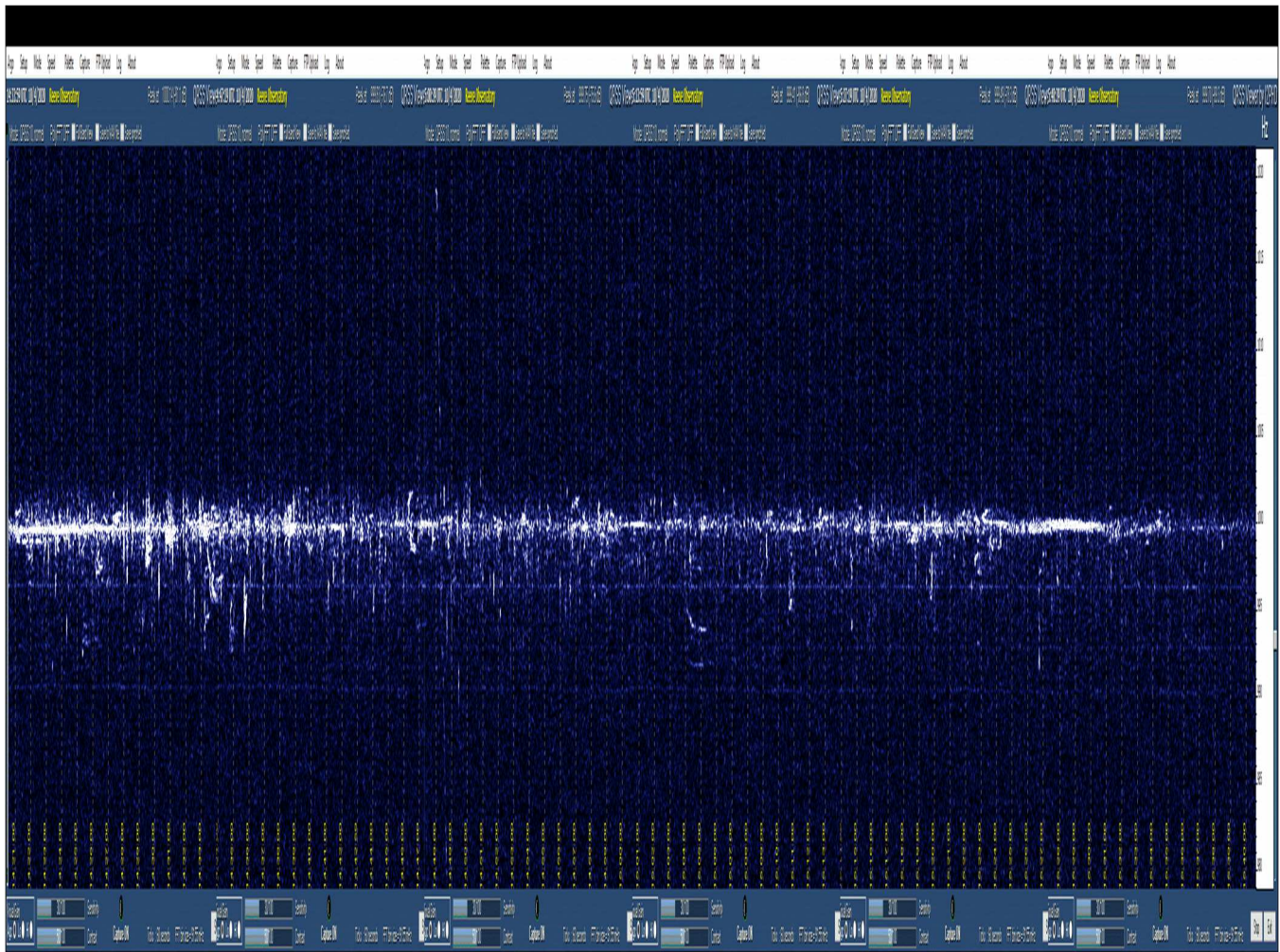


Figure 27 ~ Six images at 15 MHz for 4 October from 1421 to 1540 and spanning 79 min. In this series, the received signal just started to be detectable at 1421 and almost immediately the number of meteor trail reflections that are detected is relatively high. However, by the end of the series at 1540, both the signal level and number of echoes has decreased considerably.

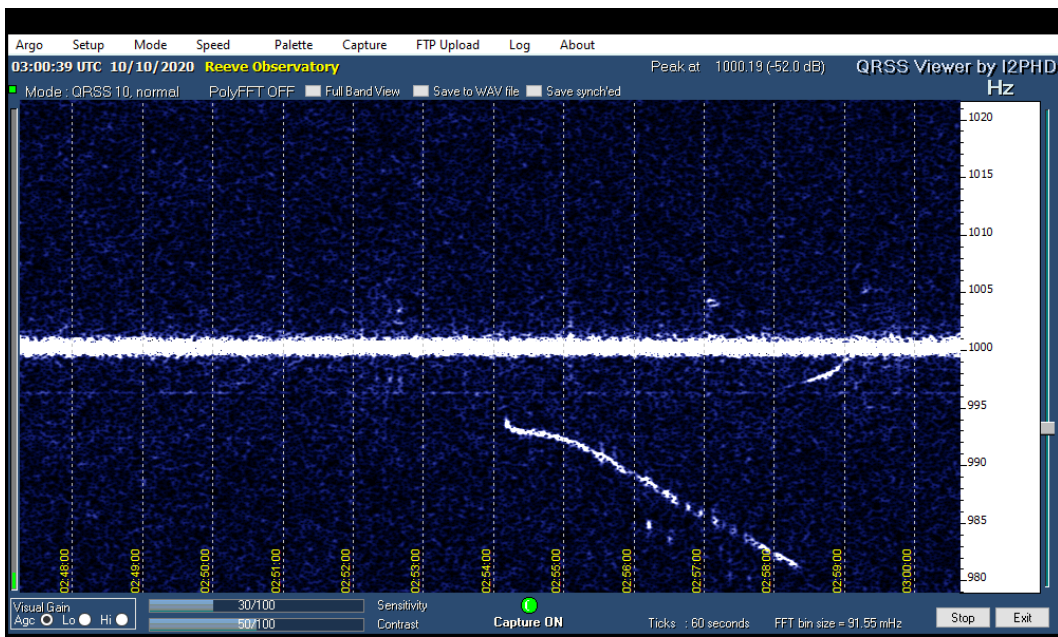


Figure 28 ~ Spectra at 15 MHz for 10 October from 0248 to 0300 with unusual negative going frequency sweep feature starting at 0254 and appearing to shift and reverse to positive going between 0258 and 0259. However, the end of the first event and beginning of second event may be coincidental.

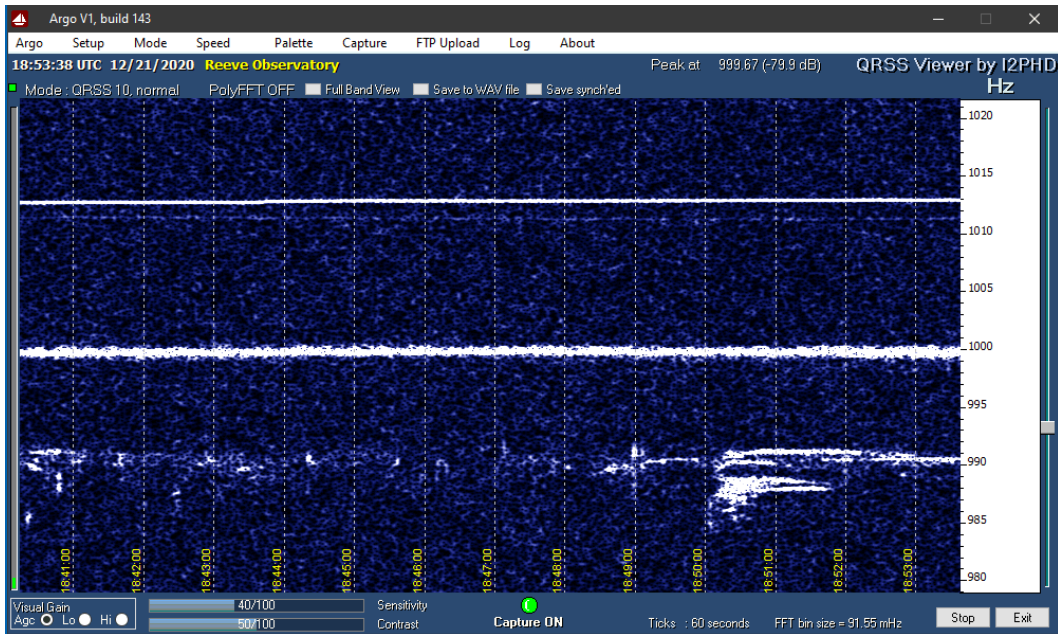


Figure 29 ~ Dual frequency record from 1840 to 1853 on 21 December 2020. The carrier frequencies were 15 MHz for the trace at 1000 Hz and 25 MHz for the trace at 990 Hz. The trace at 1013 Hz is spurious. A long-duration echo is seen at 1850 on the 25 MHz trace as are a few short-duration echoes. The long-duration trace has at least two striations with negative frequency shift and one with a small positive frequency shift lasting almost 3 min.

## 6. Conclusions

I have shown that the HF transmissions from the time-frequency stations WWV and WWVH, both about 4000 km away, can be reflected by meteor trails and detected at Anchorage, Alaska. The concept of virtual transmitters, located at ground reflection or ionospheric refraction points in the propagation paths from the transmitting stations to the receiver, is used to explain reflections of the distant transmissions from meteor trails.

The demodulated audio during meteor activity consisted of short tone bursts or tone enhancements, some with a bell sound. Long duration bursts had a wavering tone if the Doppler frequency shift was more than a few Hz. Doppler shifts as high as 10 Hz were observed, with some exceptional echoes reaching much higher values. When large numbers of short-duration echoes were being received, they generally favored one frequency shift polarity. The displayed echoes showed an increase of 10 to 20 dB over the background noise level.

Almost all detections occurred between 4:00 am and 9:00 am local solar times. Detections were limited more by propagation conditions than by the number of meteor trails. Both underdense and overdense meteor trail reflections were detected, as inferred by their short and long durations, respectively.

A surprisingly high number of long-duration echoes were detected, lasting up to 7 min, and many of these were striated. Short duration echoes greatly outnumbered long duration echoes. Many short duration echoes were detected as streams. Continuous streams were observed in January and September 2020 lasting 1.5 h. Although meteor showers probably contributed to streams, such as the Quadrantids in January, propagation conditions determined when and for how long the streams were detected.

---

## 7. References and Weblinks

- [Bourdillon] Bourdillon, A., Haldoupis, C., Hanuise, C., Le Roux, Y., and Menard, J. (2005), Long Duration Meteor Echoes Characterized by Doppler Spectrum Bifurcation, *Geophysical Research Letters*, 32, L05805, doi: 10.1029/2004GL021685, available at:  
<https://agupubs.onlinelibrary.wiley.com/doi/10.1029/2004GL021685>
- [Goodman] Goodman, J., Meteor Burst Communications, *The Froehlich/Kent Encyclopedia of Telecommunications*, Vol. 10, 1995
- [Duprat] Duprat, J., C. Engrand, Maurette, M., Kurat, G., Gounelle, and M., Hammer, C., Micrometeorites from Central Antarctic snow: The CONCORDIA collection, *Advances in Space Research* 39 (2007) 605–611
- [McKinley] McKinley, D., *Meteor Science and Engineering*, McGraw-Hill Book Co., 1961
- [Reeve15-1] Reeve, W., Sudden Frequency Deviations Caused by Solar Flares: Part I ~ Concepts, 2015, available at:  
[http://www.reeve.com/Documents/Articles%20Papers/Propagation%20Anomalies/Reeve\\_SuddenFreqDevConcepts\\_P1.pdf](http://www.reeve.com/Documents/Articles%20Papers/Propagation%20Anomalies/Reeve_SuddenFreqDevConcepts_P1.pdf)
- [Reeve15-2] Reeve, W., Sudden Frequency Deviations Caused by Solar Flares: Part II ~ Instrumentation and Observations, 2015, available at:

[http://www.reeve.com/Documents/Articles%20Papers/Propagation%20Anomalies/Reeve\\_SuddenFreqDevMeas\\_P2.pdf](http://www.reeve.com/Documents/Articles%20Papers/Propagation%20Anomalies/Reeve_SuddenFreqDevMeas_P2.pdf)

{Reeve-IDC} Ionosphere-Distance Calculations, 2020, available at:

[http://www.reeve.com/Documents/Articles%20Papers/Reeve\\_Ionosphere-DistanceCalc.pdf](http://www.reeve.com/Documents/Articles%20Papers/Reeve_Ionosphere-DistanceCalc.pdf)

[Schanker] Schanker, J., Meteor Burst Communications, Artech House, 1990

[Sugar] Sugar, G., Radio Propagation by Reflection from Meteor Trails, Proceedings of the IEEE, February 1964

{Argo} <https://www.i2phd.org/argo/index.html>

{GCMap} <http://www.gcmap.com/mapui?P=FNL-anc-bkh>

{IMOMC} <https://www.imo.net/resources/calendar/>

{LiveMeteor} <http://www.livemetears.com/>

{MDCIAU} [https://www.ta3.sk/IAUC22DB/MDC2007/Roje/roje\\_lista.php](https://www.ta3.sk/IAUC22DB/MDC2007/Roje/roje_lista.php)

{Meteor} [http://www.reeve.com/Meteor/Meteor\\_simple.html](http://www.reeve.com/Meteor/Meteor_simple.html)

{MetNews} <https://www.meteornews.net/category/news/>

{Roswell} <http://roswellmeteor.com/>



**Author:** Whitham Reeve obtained B.S. and M.S. degrees in Electrical Engineering at University of Alaska Fairbanks, USA. He worked as a professional engineer and engineering firm owner/operator in the airline and telecommunications industries for more than 40 years and now manufactures electronic equipment used in radio astronomy. He also is a part-time space weather advisor for the High-frequency Active Auroral Research Program (HAARP) and a member of the HAARP Advisory Committee. He has lived in Anchorage, Alaska his entire life. Email contact: [whitreeve@gmail.com](mailto:whitreeve@gmail.com)

---

## Document Information

Author: Whitham D. Reeve

Copyright: © 2021 W. Reeve

Revisions: 0.0 (Original draft started, 11 Apr 2019)  
0.1 (Narrowed scope to meteor trail reflections, 31 Dec 2020)  
0.2 (Completed draft of concepts, 1 Jan 2021)  
0.3 (Added Argo images, 5 Jan 2021)  
0.4 (Completed 1<sup>st</sup> draft, 8 Jan 2021)  
0.5 (Added more Argo images, refined captions, 11 Jan 2021)  
0.6 (Added details to section 2, 19 Jan 2021)  
0.7 (Added escape velocity description, revised eq. numbering, 20 Jan 2021)  
0.8 (Added to audio and spectra descriptions, 23 Jan 2021)  
0.9 (Additional info in Introduction, 25 Jan 2021)  
1.0 (Completed 2<sup>nd</sup> draft, 17 Mar 2021)  
1.1 (Distribution, 03 Jun 2021)  
1.2 (Added quantity reaching surface & converted to .docx, 15 Jul 2021)

Word count: 8193

File size (bytes): 17838264